THE HYDRODYNAMIC EFFECTS OF LARGE VESSELS ON RIGHT WHALES

Amy R. Knowlton[1], F. Thomas Korsmeyer[2], Justin E. Kerwin[2],
Hua-Yang Wu[2], and Brodie Hynes[2]

[1] New England Aquarium
Central Wharf
Boston, MA 02110

[2] Department of Ocean Engineering
Massachusetts Institute of Technology
Cambridge, MA 02139

Final Report

March, 1995

In fulfillment of Contract No. 40EANFF400534

National Marine Fisheries Service
Northeast Fisheries Science Center
166 Water Street
Woods Hole, MA 02543

THE HYDRODYNAMIC EFFECTS OF LARGE VESSELS ON RIGHT WHALES

Table of Contents

EXECUTIVE SUMMARY

The North Atlantic right whale species *(Eubalaena glacialis)* is severely endangered with less than 350 animals remaining in the western North Atlantic. Collisions from large vessels represent the highest source of anthropogenic mortality for this species and may be impacting their ability to recover. However, little is known regarding the effects of large ships on whales and the nature of these collisions.

It is well documented in the shipping world that two ships operating in proximity induce hydrodynamic forces on each other which can lead to collisions. The purpose of this research study was to ascertain whether a large vessel in transit could create hydrodynamic forces which could draw in a right whale resulting in possible injury or mortality.

A secondary aspect of this research was to evaluate the propeller wounds on a dead right whale from a known vessel to determine the feasibility of calculating propeller diameter from measurements of the wounds, and in turn, determining the size of the vessel involved in the collision.

For this project, an existing computer program, which computes the forces created by pressure fields as the water moves around the ship's hull, was extended to include the calculation of the rigid-body motion of the whale due to the hydrodynamic forces. This allowed us to simulate the movement of the whale in relation to a passing ship.

The three forces imposed on a whale by a passing ship which are modeled by the program are sway, surge and yaw. Sway is the lateral force, surge is the longitudinal force, and yaw is the horizontal moment. In general, these forces increase with the square of the ship speed, and increase as water depth decreases. The force calculations are presented for three vessel types: a 148 meter Mariner class container ship, a 191 meter Panamax tanker, and a 300 meter SL-7 class container ship. At a given ship speed, the Panamax, the bluffest ship, induces the largest forces, and the SL-7, the finest of the three, induces the smallest. Simulations of whale motion induced by the passing ships are shown using the Mariner class vessel, a whale of 15 meters length and 3 meter beam, and a water depth of 12.9 meters. The whale is held fixed at 5.5 meters below the surface at

a position initially parallel to the approaching ship and at varying offsets from the side of the vessel. The ship speed is constant. No modeling of whale behavior is included in these simulations.

The cases simulated are for lateral offsets of -0.5, 1.0, and 7.0 whale beams, the separation from the side of the whale to the side of the vessel. In all three cases, the initial positive sway force induced by the passing bow pushes the whale away from the ship. The subsequent negative sway force draws the whale in towards the ship's path but the whale arrives in the path after the ship has passed by. At the -0.5 offset, the whale is nearly struck by the ship, so we assume that any position inside of -0.5 whale beam (or 1.5 meters inside of the ship's beam which is approximately 21 meters) would result in a collision. A fourth simulation models a situation where a whale surfaces in proximity to a passing ship and is not exposed to the initial positive sway force. In this case, at one whale beam from the ship, the whale is drawn into the ship. The maximum distance at which a whale could be drawn has not been determined. This probably depends on the water depth.

The analyses to determine propeller diameter are problematic. The first technique which measures the length and depth of the cuts results in an inaccurate result from a known situation. This is because the surface contour of the whale is not known during the propeller interaction and so the measurements relate to an unknown geometry.

The second technique uses the characteristics of a particular vessel (speed, propeller RPM, propeller diameter, and number of blades) to determine whether the spacing between the propeller cuts corresponds to the ship in question. If the location and date of the strike is known, it might be possible to identify ship traffic for that period and use their characteristics to narrow down which ships may have been involved. Neither technique would allow you to determine the actual vessel involved with certainty.

Additional modeling efforts could be carried out to simulate other types of vessels, determine at what distance an "appearing" whale can be drawn in to a passing ship, and evaluate whether ships are more dangerous to whales in shallow waters. Whale behavior should be included in any further modeling efforts. Inclusion of whale behavior might allow us to determine whether slowing vessels would reduce the chances of hitting a whale.

INTRODUCTION

The North Atlantic right whale *(Eubalaena glacialis)* is considered the most endangered large whale in the world. Less than 350 remain in the North Atlantic and their future is considered tenuous (Knowlton *et al.* 1994). Right whales are primarily a coastal species with all five of their presently identified seasonal habitats lying within 40 miles of the coast. This feature makes them susceptible to a high incidence of interactions with human activities, such as shipping. Mortalities and severe injuries from large ships have occurred and represent nearly one third of all documented mortalities (Kraus 1990; Kenney and Kraus 1993). In order to maximize the recovery of this severely endangered species, measures to mitigate these interactions must be addressed. The Final Recovery Plan for the Northern Right Whale (NMFS 1991) lists the reduction of human-caused mortalities as the number one priority needed to move the species towards recovery. Objective 1 of the Recovery Plan specifically outlines the steps necessary for addressing the problem of ship strikes. For reduction of ship strikes, the Plan states a need to "educate mariners about northern right whales" as well as to "implement appropriate controls on ship operation and design."

In an attempt to understand the effect of large ships on whales more clearly, so as to move towards developing a policy regarding ship operations in right whale habitats, a collaborative effort was initiated between the New England Aquarium and the Ocean Engineering Department at the Massachusetts Institute of Technology. A goal of the research was to determine through computer modeling whether a whale can be drawn in to a vessel as a result of hydrodynamic forces, and, if so, under what circumstances this might occur. In addition, since it is

rarely known in a ship/whale collision what size vessel was involved, situations where the length and depth of propeller cuts can be measured on stranded or live whales can provide insight into the propeller diameter of the vessel thereby providing a rough estimate of the size of the vessel involved. This technique is applied to an incident of a ship/whale collision where all the parameters were known to determine its potential effectiveness when evaluating future stranding events.

With both these analyses, we hope to provide the reader with more insight into how ships affect whales. Yet, it is just a starting point and clearly, much more needs to be done to understand further the ship/whale interactions, and in turn, develop strategies which could minimize collisions.

SHIP CHARACTERIZATION STUDY

Overview

The report by Hain *et al.* (1994) describes the results obtained from recording the shipping traffic accessing ports whose channels transect the only known calving ground for the North Atlantic right whale. The two channels targeted for the study were the St. John's channel---the entrance to the Port of Jacksonville and the Mayport Naval base, and the St. Mary's channel---the entrance to the Port of Fernandina Beach and the Kings Bay Naval Submarine Base. Human observers situated at land-based locations at the channel entrances recorded data (date, time, site, vessel category, vessel type, and direction of travel (inbound or outbound)) during the month of January 1993 for nearly all of the ships entering and exiting each channel during daylight hours. At night, the data was taken from the log

books of the pilot associations, which are assumed to reflect approximately 60% of the commercial traffic through each channel.

Vessel Size and Important Vessels

Based on Hain *et al. 's* (1994) data, the length of the average piloted vessel is 590 feet with a standard deviation of 145 feet; the smallest being a 144-ft coastal tanker and the largest, several 950-ft container ships. Vessels worthy of hydrodynamic investigation are those which pose the greatest threat to the whales. These vessels might be the ones which are most common in the winter migration grounds. From Table 2 in the original report, the most common vessel type is recreational. While they are the most common vessel type the report reasoned that this class of vessel does not pose as great a threat as the classes of larger vessels. The next largest class is the container ship and after that, car carriers. The aforementioned study proved to be very useful in the determination of vessels which should be examined for their hydrodynamic effects on whales. The vessel types considered are:

Container Ship

Car Carrier or Tanker

Extreme Size Container Ship or Tanker (Max. Port Capacity)

For the dimensions of the car carrier, tanker, and container ship, the Lloyd's Ship Registry has been consulted for the specifications (length, beam, draft) of named vessels.

The vessels modeled in the simulations are:

Mariner Class: Container Ship

Length: 148.37 m

Beam: 20.76 m

Draft: 6.732 m

Panamax: Tanker

Length: 190.51 m

Beam: 29.27 m

Draft: 11.307 m

SL-7: Extreme Case

Length: 300 m

Beam: 36.0486 m

Draft: 11.592 m

Figures 1 through 3 show the geometry of these ships in wire-frame plots. The mesh density which is shown is that used in the hydrodynamic computations.

The Coast Guard Cutter Point Francis

The 82-foot Coast Guard Cutter Point Francis might appear to be a candidate for this hydrodynamic study as it is the one case where a specific ship is known to have hit a right whale. More specifically, the Point Francis hit a 1-2 month old calf 3 miles offshore and 7 miles north of St. Augustine, FL in January, 1993. The

vessel was operating at a cruising speed of 10 to 15 knots when it hit the calf and personnel aboard the vessel did not see the animal before it was struck (as reported by U.S. Coast Guard). The lesions on the whale are described in the necropsy report (USFWS 1993):

> Two distinct and separate propeller laceration series were evident on the body. The first extending from the dorsal peduncle and terminating just behind the cranium and the second entering along the lower left flank and running down to the ventral throat and head. ... Evidence from the entry and exit sites of each individual slash indicate that the animal was struck from behind as the blades traveled up the body towards the head.

The fact that the whale was overtaken from behind and was approximately equally lacerated by both propellers suggests that the whale was directly in the path of the ship. The hydrodynamic aspects of such an encounter would seem to be irrelevant unless the surge force on the whale were large enough to actually prevent a collision. Apparently this was not the case. Therefore, no efforts were directed towards discretizing the Pt. Francis hull. This incident is of value, however, in confirming equations which could be utilized to determine propeller size when the dimensions of the cuts on the whale are known. These equations are described in a later section on propeller analyses.

NORMALIZATION OF WHALE MEASUREMENTS TO CREATE THE AVERAGE RIGHT WHALE

In order to perform simulations involving a right whale, an accurate geometric representation of the whale was developed. The data used to describe a typical right whale *(Eubalaena glacialis)* were obtained from measurement data collected

by Omura *et al.* (1969) of North Pacific right whales. This data set was chosen as it contains consistently collected measurements for numerous right whales. A whale length of 15 meters was chosen for the simulations in this report. This represents a North Atlantic right whale of adult age.

The following data were normalized with respect to the total length of the whale:

Tail flukes, total spread
Flipper, greatest width
Circumferences at: front of flipper, umbilicus, anus, and caudal terminus
Depths of Body: middle insertion of flipper, anterior insertion of flipper and umbilicus.

A linear least squares approximation was then fit to the data providing equations for each of the geometric parameters as a function of the whale length. The raw data were also averaged to find the geometric description of the average whale:

Whale: *Eubalaena glacialis*

Length: 15 m
Beam: 3.08 m
Draft: 3 m

The averaged data were then used with a CAD program to produce a geometric data file for the right whale which conforms to the hydrodynamic code input format. This geometric model is shown in Figures 4 through 7. Note that the model does not have fins or flukes. The lifting effects of such surfaces are not

included in the hydrodynamic model as their contribution to the non-lifting flow is negligible, so their inclusion is not warranted.

Appendix 1 describes the equations of linear least-squares fits.

SHIP/WHALE HYDRODYNAMICS

Introduction

Two ships operating in proximity induce hydrodynamic forces (we use the term "forces" in a generalized sense which includes moments) on each other which can have serious consequences. In unrestricted waters these forces can lead to collisions and in restricted waters they can also lead to groundings and damage to shore-based structures. The forces under consideration here are not due to free-surface waves, but rather the pressure fields produced by the fluid having to move around the ship hull under a waveless free surface. This is an approximation which becomes exact in the zero-speed limit. For cases of interest, in water of restricted width and/or depth where speeds are low, these forces are more important than the free-surface wave forces and this model is appropriate. Traditionally, the computation of these forces was done with strip theory or slender-body theory. Recently, however, the development of a fully three-dimensional theory and implementation on high-performance workstations has been completed (Korsmeyer *et al.* 1993).

This project makes use of this capability, intended for ship interactions, to analyze the hydrodynamic effects induced on right whales by passing ships. In addition, this project extends the computational capability to include the calculation of the

rigid-body motion of the whale due to the hydrodynamic forces.

A key feature in this extension is the method for the computation of the forces in the general case that both bodies may be moving. This method combines the use of Bernoulli's equation with Lagrangian analysis and uses the concept of virtual motion. A derivation of the expression for the forces is found in Appendix 1. The inclusion of the force due to the flow induced by the ship propeller is provided by actuator disk theory as outlined in Appendix 2.

Forces are usually reported in the form of nondimensional coefficients, as defined in Appendix 2. This is because for this model the forces depend on the physical parameters of the problem in a straightforward manner. Given a ship hull form, a whale form, and a water depth, the forces as a function of relative ship and whale position may be reduced to a single curve for each force if the forces are normalized by: water density; a representative length, which we take to be the ship

length raised to an appropriate power; and the square of the ship speed. This means that when considering a plot of the coefficient of the force on a whale as it is passed by a ship, the actual value of the force may be computed for any ship speed simply by multiplying the coefficient by the normalizing parameters in consistent units. When considering the simulations of a whale moving under the hydrodynamic forces induced by a passing ship, there is no need to dimensionalize, as the relative positions of the ship and whale will not change.

The forces on the whale are reported in a reference frame fixed to the whale, for which the x-axis points in the direction of the nose, the y-axis points to port, and

the z-axis points upward. The surge force is in the x-direction, the sway force is in the y-direction, and the yaw moment is about the z-axis as shown in Figure 8.

Convergence Studies

The computer program used in this project was developed to study the interaction of ships. Convergence studies which establish the fineness of the spatial and temporal discretizations required for accurate results for ship interactions may be reviewed in Korsmeyer *et al.* (1993). In this case, where we are interested in the analysis of the interaction of a ship with a whale, the disparate sizes of the two bodies suggests that the spatial convergence be established for this specific case. This is because panel-method experience indicates that nearby panels not be markedly different in size, and the ship and whale panels may indeed be close, yet accurate geometric modeling of the bodies leads to panels which are considerably smaller for the whale than for the ship. Correcting this by using similarly small panels on the ship leads to computational burdens which are beyond the resources of this project. Some convergence studies are required then to find acceptable discretizations, balancing accuracy with efficiency.

We are interested in modeling a finite-depth environment of effectively infinite width, so another convergence study is done to pick a finite computational width which accurately models the effectively infinite width of interest.

All of the convergence studies are done with the ship moving in a prescribed manner (constant velocity) while the whale is held at a constant position. This simplification does not affect the conclusions of the convergence studies while it

reduces the required computational effort. A further simplification is that the ship is replaced by an ovoid (see Figure 9) so that the discretization may be changed easily. We are not interested in the forces on ship 1, as its motion is prescribed a priori so we report only the forces on the whale.

The forces on the whale considering various parameters are explained in the following sections and depicted visually in Figures 11 through 34. In these figures the x-axis, Offset, represents the longitudinal offset of the whale from the mid-length of the ship (Figure 10). At 0 longitudinal offset, the mid-length of the whale coincides with the mid-length of the ship. The ships length equals 1, therefore the ships bow is at 0.5 and the ships stern is at -0.5. The surge, sway, and yaw coefficients or forces on the whale at the given parameters are displayed in these figures. For example, in Figure 11, a strong surge coefficient pushing the whale in a forward direction is apparent at a longitudinal offset of approximately 0.4, as the bow of the ship is passing the whale. At offset -0.4, this coefficient is negative. Therefore the whale is being pulled backwards as the stern of the ship passes by. Likewise, in Figure 12, the sway coefficient representing the forces pushing the whale towards or away from the side of the vessel is positively highest as the bow and stern of the vessel pass. The negative coefficient, which would draw the whale towards the ship is the highest at approximately 0.2 and -0.2 longitudinal offset, or near the middle of the passing ship. In Figure 13 which represents the yaw coefficient, at approximately 0.2 longitudinal offset, forces imposed would tend to angle the nose of the whale towards the ship and at -0.2 the forces would angle the whale away from the ship. The significance of these figures is explained in the following sections.

Convergence Study For Spatial Discretization

Figures 11 through 13 show the convergence study for spatial discretization for the surge and sway forces and the yaw moment. In this study the ship is moved with constant velocity past a fixed whale with a separation between them of one whale beam (side of the whale to side of the ship)(Figure 10). A small separation distance tends to make convergence more difficult. We can probably pick a separation distance small enough for any discretization such that convergence is too computationally burdensome to demonstrate. A one whale beam separation is a practical choice for this study. The number of panels on the ovoid and on the whale is doubled twice for each body. It is apparent that for all three quantities convergence to graphical accuracy is achieved with as few as 400 panels on the ship and 100 panels on the whale.

Since we can afford the added computational effort, and we know that it will provide convergence at still smaller separation distances, we actually use 400 panels on the ships and 196 panels on the whale in all cases in this study. Figures 1 through 9 show all of the discretizations used in the hydrodynamic analyses.

Convergence Study For Channel Width

This convergence study is required because the area we are modeling where right whales and ships interact is of finite depth but not width. The rectangular channel Green function subroutine which is used in the computer code requires a finite width to the restricted water. This width may indeed be large, so long as it is

finite. The point of this study is to select a finite width which is effectively infinite. The study is conducted with a 300 meter SL-7 hull in a channel of depth 12.9 meters, and a channel width varying from 5 to 125 ship beams (one ship beam equals 36 meters), with data points at 5, 10, 25, 50, and 125 ship beams. The ship is placed in the center of the channel for each simulation; the whale is placed 15 meters from the ship. Figures 14 through 16 show how the forces and moments are reduced as the width of the channel is increased, but beyond about 25 ship beams the increase no longer has any effect as the channel is effectively infinitely wide. From these results we select a channel width of 50 ship beams for all of the cases in this study.

Forces induced on a whale by a passing ship with the whale held fixed

Figures 17 through 40 present results from simulations in which each of the three ships is passing the whale while it is held fixed at 5.5 meters below the surface (surface to top of whale). The point of these simulations is to show how the hydrodynamic forces and moments on the whale vary as a function of water depth, ship type, and proximity. The forces and moments are usually presented in the form of non-dimensional coefficients. These coefficients are defined in Equations 8 though 34 in Appendix 2. Note that part of the non-dimensionalization is the square of the ship speed. Hence the plots of the coefficients are independent of ship speed and the actual forces and moments scale like the speed squared (that is, a doubling of the ship speed yields a four-fold increase in the dimensional force or moment).

These results show that the shallower water depth increases the maximum force

values. They also show that the finest of the three ships, the SL-7, induces the smallest force coefficients and the bluffest, the Panamax, usually induces the largest. The actual force values induced in actuality may well not follow these trends, however, as they depend on the square of the ship speed and in general finer ships are designed for higher speeds than bluff ships.

The summary plots, Figures 35 through 40, show how the maximum values of the forces depend on the separation of the ship and whale for each of the three ships. These plots are dimensional so that the different ships may be directly compared. The plots are of the maximum force value obtained as the simulation of each ship passing a fixed whale (at the indicated lateral offset) is computed. Note that the dimensionalization of the computed coefficients is carried out with the same speed for all ships: 15 knots. As might be expected, when the lateral offset of the whale from the ship is small, the bluffest ship, the Panamax, produces the largest forces on the whale.

The Simulation of a Ship Passing a Whale

The expression for the forces on the whale when the whale is allowed to move which is derived in the Appendix 2 is incorporated into the ship interaction code so that simulations are run with the whale position changing due to the hydrodynamic force. In addition, as outlined in Appendix 3, the flow due to a simple propeller model is included. The motion of the ship is prescribed to be a constant forward speed. The whale is free to move horizontally under the action of the forces (vertical forces were not computed in this model) and there are no other forces applied to the whale. The latter makes reference to the fact that there

is no attempt to model supposed whale behavior. It is important to note that since there is no whale behavior modeled in these cases, the relative motions of the two bodies are speed independent. Only if forces on the whale which do not scale with the ship speed were included would ship speed become an issue. This is obviously the case if some type of whale behavior is modeled, as the force that the whale could generate to escape the ship (supposing that that is what whales attempt to do) is not dependent on the ship speed.

Several simulations are shown in Figures 41 through 52. In all cases, the ship used in the simulations is the Mariner hull and the water depth is 12.9 meters. For each simulation, the forces on the whale are reported, followed by the relative positions of the ship and whale as the ship passes the initial position of the whale, and finally a close-up of the whale position is shown.

The first three simulations are of a ship over taking a whale which is aligned parallel to the ship track, initially at various lateral offsets from the ship. These lateral offsets are measurements from the side of the whale to the side of the ship, so they are the clearance which would be between the ship and the whale if the whale were held fixed as in the above section. The cases simulated were for lateral offsets of -0.5, 1.0, 7.0 whale beams (Figures 41 through 49). Note that in the first case, if the whale were held fixed the ship would necessarily hit the whale.

It is very interesting to note that in none of these cases, including the case of the initial lateral offset of -0.5 did the ship hit the whale. In all cases, the initial sway force, which tends to push the whale away from the ship, is sufficient to accelerate the whale so that when the effect of the much greater suction force due to the ship

and propeller is felt, the inertia of the whale is great enough that the whale does not cross the ship track until after the ship has passed. In the case of the initial lateral offset of -0.5, the whale passes close enough to the ship it is likely that the ship will hit the whale for any offset which initially positions the whale closer to the ship centerline.

A final simulation shown in Figures 50 through 52 is an attempt to model the case of a whale approaching the free surface in the presence of a moving ship. This is carried out by bringing the whale into existence in the proximity of the ship. Such an event might occur, for example, if a whale is surfacing from depth. In this case the simulation is started with the ship at the longitudinal -0.2 offset position, with the lateral offset at 1.0 whale beam. In this case, the ship hits the whale.

RELATIONSHIP BETWEEN PROPELLER CONTACT MARKS ON WHALE AND PROPELLER DIAMETER

Necropsy reports of marine mammals struck by propellers ideally report the dimensions of the lacerations. The necropsy report on the right whale struck by the Coast Guard Cutter Point Francis reports the distance between the parallel lacerations or contact marks, their length and their depth (USFWS 1993).

We would like to be able to deduce as much information as possible about the ship which has caused the lacerations from the laceration measurements. Two approaches are possible. One is to deduce the propeller diameter from the length and depth of the lacerations, the other is to deduce the combination of ship speed, propeller diameter, propeller RPMs, and number of propeller blades which

correspond to the distance between the lacerations. Note that in either case there is no way to absolutely identify a particular ship from the data in a necropsy report.

For the first method, we label the length of the laceration l, and the depth of the laceration d. We make the assumption that these dimensions describe the arc of a circle with diameter equal to that of the propeller in that l is the chord which subtends the arc of height d. Then the diameter of the circle, and therefore of the propeller is

$$D = (d^2 + l^2/4) / d.$$

The problem with this method is that the assumption is not well supported. There is no way to know what the shape of the whale body surface is as it interacts with the propeller blade. It probably deflects and distorts, and probably does so differently for different styles and sizes of propellers. Application of this formula to the data in the necropsy report cited above suggests that the lacerations were made with a propeller with a diameter of 2.3 ft. while the correct result is 3.5 ft. To obtain the 2.3 ft. result we averaged the computed results for the reported lacerations, not including the shallowest three of them. This method appears to be unreliable.

Propeller diameters range between 3 to 5% of the total length of the vessel, depending on the vessel type. Propeller sizes on large tankers and containerships range from 3 to 3.5 % of the vessel length, or 6 to 8 meters in diameter. On large oceanographic ships and large fishing vessels, propeller sizes are about 5% of the length, or 3 to 4 meters in diameter. On high speed vessels such as Coast Guard

cutters or mega yachts, the propellers are approximately 4.5% of the length, or 1 to 2 meters in diameter. Slower speed, small fishing vessels also have propellers of this diameter.

For the second method, we label this distance between the laceration scars h. If we assume that a whale is struck by the tips of a relatively large propeller, the contact with the whale will be in the direction of the relative motion between the blade tip and the whale. The pitch of the propeller will not be relevant. Assume, for the moment, that the whale speed is negligible compared with the tip speed of the propeller. Take a local coordinate system with the x axis in the direction of motion of the ship, and the y axis to starboard. Then, the path of the tip is

$$\begin{aligned} x(t) &= V_s t \\ y(t) &= \pi n D t \end{aligned} \tag{1}$$

where V_s is the ship speed in feet per second, t is time in seconds, n is the propeller speed in revolutions per second and D is the propeller diameter in feet. The absolute path of the blade tip makes an angle

$$\beta_t = \tan^{-1} \frac{V_s}{\pi n D} \tag{2}$$

The next blade lags the first one by a time

$$T_b = \frac{1}{Zn} \tag{3}$$

where Z is the number of blades. The spacing between contact lines, measured in the direction of motion of the ship, will therefore be

$$V_s T_b = \frac{V_s}{Zn} \tag{4}$$

and the spacing normal to the lines of contact will be

$$h = \frac{V_s}{Zn} \cos\beta_t = \frac{\pi V_s D}{Z\sqrt{V_s^2 + (\pi n D)^2}} \tag{5}$$

This can be put in terms of ship speed in knots, V_{sk} and propeller RPM, N as follows,

$$h = \frac{\pi V_{sk} D}{Z\sqrt{V_{sk}^2 + 0.00096 N^2 D^2}} \tag{6}$$

Use of this equation can be illustrated by the example of the 82 foot Coast Guard Cutter Point Francis although there is some discrepency between the speed and RPMs reported in the ships log (provided by the U.S. Coast Guard) and the information collected directly from the commanding officer. The commanding officer stated the speed of the cutter at the time of the collision was approximately 10 knots, and the propeller RPM was 320 (personal communication, Lt. Burke, US Coast Guard). The propeller diameter is 3.5 feet, and the propeller has 5 blades. Equation 6 yields a value of h of 0.63 ft (19.2 cm). This agrees very closely with the results of the necropsy examination report of 10 January 1993, where the average value of h is 19 cm. The ships' log reports that the cutter was making turns for 15 knots at 600 RPMs. This results in an h value of 0.50 ft (15.5 cm), which does not correspond very closely with the necropsy report. At this time we are not certain which source is more accurate.

CONCLUSIONS

Hydrodynamic effects

This project has resulted in a significant advancement in the modeling of the hydrodynamic interaction of ships and nearby bodies. While the forces imposed on two ships passing in proximity are determinable in a fully three-dimensional approach (Korsmeyer *et al.* 1993), the resulting movements of the ships has not heretofore been simulated. In using this theory to try to understand how large ships affect whales, it is important that the resulting movements of the whale imposed by a passing ship be known. With the support of NMFS, this method has been developed and has provided some preliminary results regarding the ship/whale interaction question.

In the hydrodynamic analyses, the results of the simulations of one vessel type passing a passive whale, held fixed 5.5 meters below the surface at various lateral offsets from the side of the vessel, show that the whale is not drawn in to the vessel. The initial sway effect as the bow of the ship passes the whale pushes the whale away from the ship. The momentum caused by this initial force counteracts the subsequent suction forces so that, although the whale is drawn back towards the ship, it does not reach the ship's path until the ship has passed by. Even at a lateral offset of -0.5 whale beams from the side of the ship, i.e. the whale is just inside the swath of the ships path, the initial sway effect prevents the whale from being hit. In this simulation, however, the whale comes very close to being hit. Although simulations with lateral offsets inside of -0.5 whale beams from the side of the ship were not conducted, we assume that inside of the -0.5 offset, the whale would be struck. The beam of the ship used in the simulation, the Mariner class

In a situation where the whale is within the danger zone of an approaching ship, i.e. well inside the beam of the ship, the whale has three possible directions of escape, left, right or straight down. If the ship is travelling in deep water, any one of these options is a viable option which might allow the whale to get outside of the danger zone. However, if the ship is travelling in shallow water and does not have much clearance below the hull, the option of diving and going straight down may be extremely dangerous for the whale. Although vertical forces have not been integrated into this model, if a whale were placed under an approaching ship, the character of the heave force on the whale as a function of time would be similar to the sway force in the case with the whale next to the ship. Therefore, if the whale dives and clears the hull of the ship, the initial repulsive heave force would assist in increasing the depth of the whale. However if the water depth were not significantly greater than the ship depth, then the whale would be closer to the ship, with lesser velocity directed away from the ship when the attractive force began to have an effect, than is the case in the horizontal force simulations. In this case, the attractive force might be sufficient to draw the whale into the ship's propeller.

One major question that cannot be answered without including whale behavior in the hydrodynamic model is whether reducing ship speeds would reduce ship strikes with whales from a hydrodynamic perspective. A reasonable conjecture is that whales might attempt in some way to avoid a ship collision. If that were the case, then reducing ship speeds might benefit whales by reducing the hydrodynamic forces and by providing a longer reaction time to escape the danger zone. Other ways that speed reduction could provide a benefit, irrespective of hydrodynamics, are providing greater reaction time for ship operators to avoid a sighted whale and reducing the impact force if there were a collision.

Propeller Analyses

The propeller analyses described in this report may be useful in future strandings of any marine mammal species to determine the size of the vessel involved. Each analysis, however, has its limitations. The first analysis which determines propeller diameter from length and depth of the cuts was found to be inaccurate in the case of the Pt. Francis incident. Yet, if future ship/whale collisions occur with any marine mammal species where the vessel involved is known, use of this technique might allow us to determine whether the inaccuracy is consistently low.

The second analysis would require a bit more effort to determine what ship might have been involved. The Pt. Francis incident allowed us to confirm the accuracy of the equations when all factors, i.e. ship speed, propeller diameter, RPMs, and number of propeller blades, were included. Yet, as the discrepency between information sources shows in this case, accuracy of this information is important. In the event of a strike where the vessel is not known but a time and location, and measurements from the whale are known, one might be able to determine what type of ships were passing the known area at the known time. By using the characteristics for each of the ships, many ships might be ruled out. Certainly, a combination of the two techniques would be the most useful.

RECOMMENDATIONS

Any future modeling efforts should address the following factors:

1) Each vessel type is unique as to how much force it imposes on a whale. The force simulations determined for this report show that force coefficients are most affected by the ships' slenderness. It would be useful to simulate a few more ship/whale interactions using ships with larger force coefficients to determine if the

results are generally the same;

2) The modeling of the propeller forces could be more extensive as these forces do not scale with the square of the ship speed unless we assume an equilibrium propulsion point. For instance if a ship were traveling at a slow speed and the propeller RPMs were increased in order to increase the ship speed, the resulting propeller forces would be increased;

3) Modeling of vertical forces and their potential impact on a whale diving in shallow waters would be important to investigate whether a ship is more dangerous to a whale in shallow waters;

4) Additional computations to determine at what distance a whale that "appears" near a passing ship can be drawn in, and how this changes at varying water depths;

5) An integration of whale behavior into the model, with different scenarios of assumed whale behavior based on anecdotal information would allow the investigation of the effects of ship speed on the outcome of ship and whale interaction simulations.

Until whale behavior is better understood, vessel speed reductions should not be considered a definitive action that will benefit the whales based on this hydrodynamic analysis. Yet, if the evidence suggests that right whales will actively avoid approaching vessels, then vessel speed reductions should be recommended.

Efforts to mitigate ship/whale collisions should be broadened beyond just computer modeling research. While the results of this study have answered some of the questions regarding hydrodynamic effects of large ships on right whales, efforts on several other fronts should be considered and are outlined below:

1) It would be valuable to gather anecdotal information about ship strikes from ship operators. These people spend a great deal of time at sea and some have

certainly experienced the unfortunate event of striking a whale. Information regarding location of the strike and depth of the water may indicate areas where incidents are more likely to occur. Such a survey could be conducted via articles in appropriate magazines, or phone or mail interviews.

2) In a corollary to 1) ship operators could provide on the spot information on whale strikes as well as sightings. The technology exists on most ships for faxing and telephoning. An educational program to encourage ship operators to participate

would be necessary and should cover the eastern seaboard. The combined results of these two efforts might reveal whether ship/whale collisions occur more frequently in shallow water versus deep, or in certain geographic regions. Sightings data could provide information about right whale wintering grounds or other seasonal habitats.

3) A review of existing literature regarding whale reactions to ships and noise, as well as anecdotes of vessel/whale interactions may help determine how right whales are likely to behave.

4) An assessment of ship traffic along the eastern seaboard overlaid with right whale sightings and known mortalities may highlight potential problem areas.

5) Development of seasonal exclusion and/or slowdown zones in problem areas as the results of above analyses and additional computer modeling indicate with minimum economic impact to the shipping industry.

6) Field studies of the ability of acoustic devices to 'alert' right whales to an approaching ship or pilot vessel.

Efforts to address the shipping/right whale issue are underway in the southeast U.S. as well as in the Canadian habitats. In Canada, educational efforts resulted in a company doing oil drilling offshore of Nova Scotia to divert their vessels around a primary summer right whale habitat. And in the Bay of Fundy, the New

England Aquarium began a pilot project in the summer of 1994 to radio contact any large vessels transiting the Bay and request them to keep a sharp lookout for right whales. While this is just a start, it highlights the fact that education of ship personnel should be the starting point in any effort to deal with shipping in right whale habitats.

In the southeast U.S., these educational efforts are more formalized. Harbor pilots are aware of the issue and transfer this information to all ships using the three channels located in the right whale calving ground. In addition, daily aerial surveys coordinated by the New England Aquarium monitor the presence of right whales in the region and notify port personnel, military bases, as well as ships in the vicinity of any right whales (Slay *et al.* 1994). There is alot of support for this effort and awareness amongst all shipping interests has increased substantially.

Ship collisions in all areas of the right whales range could possibly be reduced with a concerted effort to educate mariners and create special zones. Computer modeling is a tool which may help us to better define these zones.

REFERENCES

Hain, J. H. W., Ellis, S.L. , and Seward, P.E. 1994. Characterization of Vessel Traffic at the St. Johns and St. Marys Channel Entrances, Northeast Florida, January 1993. NTIS 1994, Publication No. PB94-204229, National Technical Information Service, Springfield, Virginia. 56 pp.

Hough, G.R. and Ordway, D.E. 1964. The Generalized Actuator Disc, THERM Advanced Research Report No. TAR-TR6401,1964

Kenney, R.D., and Kraus, S.D. 1993. Right whale mortality - a correction and an update. Marine Mammal Science 9(4): 445-446.

Knowlton, A.R., Kraus, S.D., and Kenney, R.D. 1994. Reproduction in North Atlantic Right Whales *(Eubalaena glacialis)*. Canadian Journal of Zoology 72: 1297-1305.

Korsmeyer, F. T., Lee, C.-H., and Newman, J. N. 1993. The computation of ship interaction forces in restricted waters. Journal of Ship Research. Vol. 37, No. 4, pp. 298-306.

Kraus, S.D. 1990. Rates and potential causes of mortality in North Atlantic right whales *(Eubalaena glacialis)*. Marine Mammal Science 6(4): 278-291.

Milne-Thompson, L. M. 1955. Theoretical Hydrodynamics, 3rd Edition, Macmillan, New York.

USFWS 1993. Necropsy Examination Report: RKB-1424, *Eubalaena glacialis*, U.S. Fish and Wildlife Service, Gainesville, Florida.

Newman, J. N. 1992. The Green function for a rectangular channel. J. Engin. Maths. 26. pp. 51-59

NMFS 1991. Recovery Plan for the Northern Right Whale *(Eubalaena glacialis)*. Prepared by the Right Whale Recovery Team for the National Marine Fisheries Service, Silver Spring, MD. 86 pp.

Omura, H., Oshumi, S., Nemoto, T., Nasu, K., and Kasuya, T. 1969. Black Right Whales in the North Pacific. Sci. Rep. Whales Res. Inst., Tokyo Vol. 21, pp. 1-78.

Slay, C.K., Kraus, S.D., Conger, L.A., Knowlton, A.R., Hamilton, P.K. 1994. Aerial Surveys to Reduce Ship Collisions with Right Whales in the Nearshore Coastal Waters of Georgia and Northeast Florida. Final Report to National Marine Fisheries Service. 28 pp. + appendices.

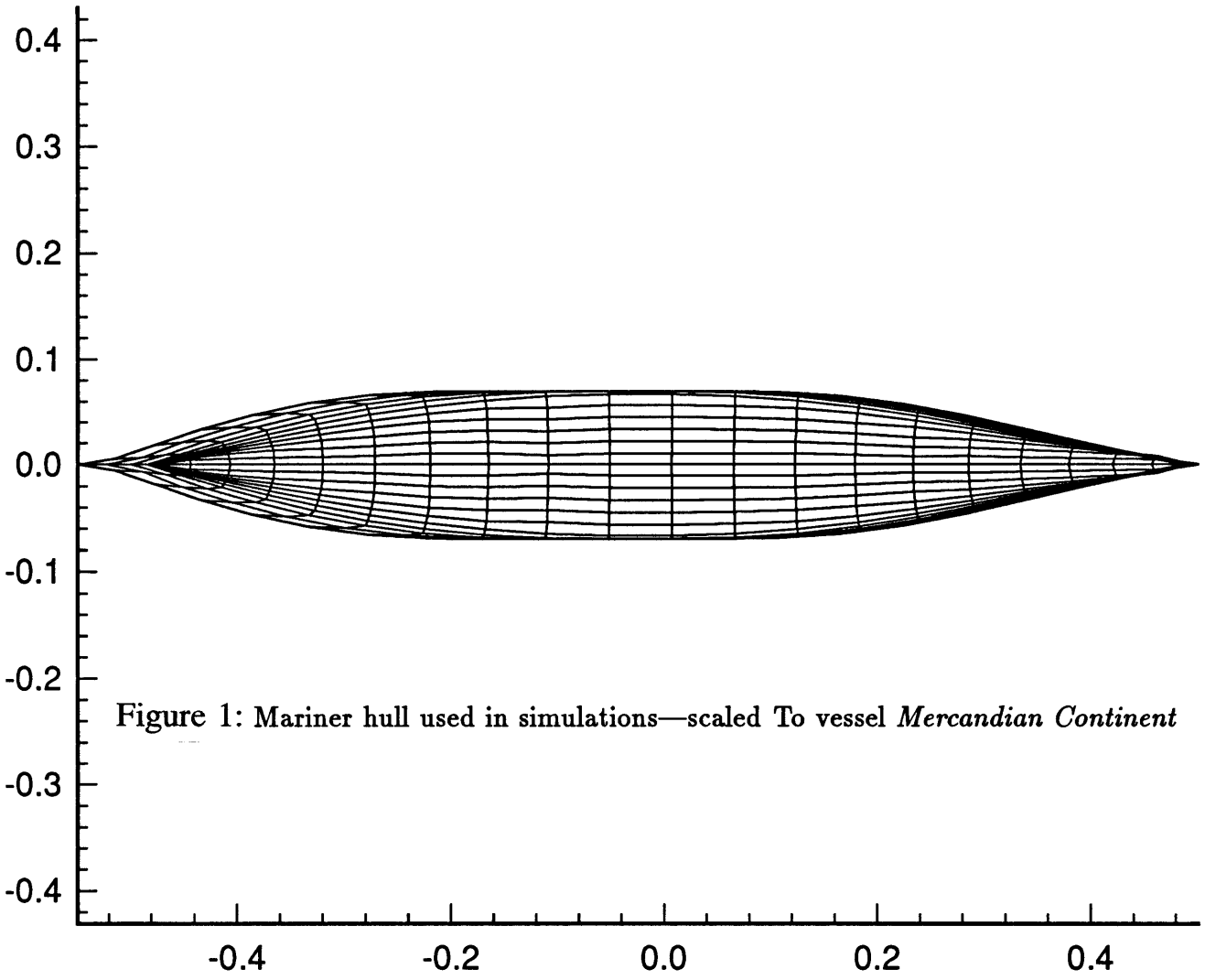

Figure 1: Mariner hull used in simulations—scaled To vessel *Mercandian Continent*

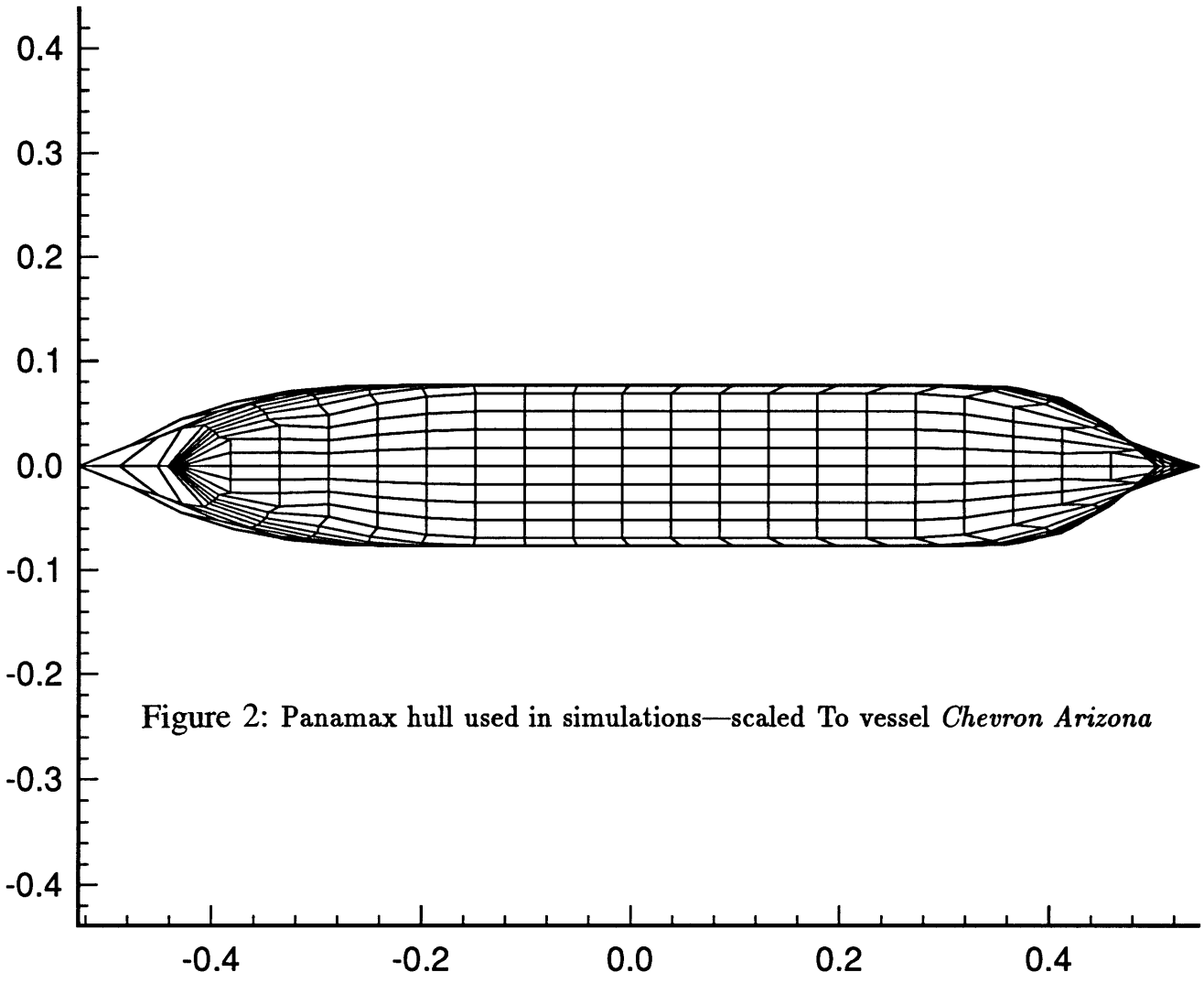

Figure 2: Panamax hull used in simulations—scaled To vessel *Chevron Arizona*

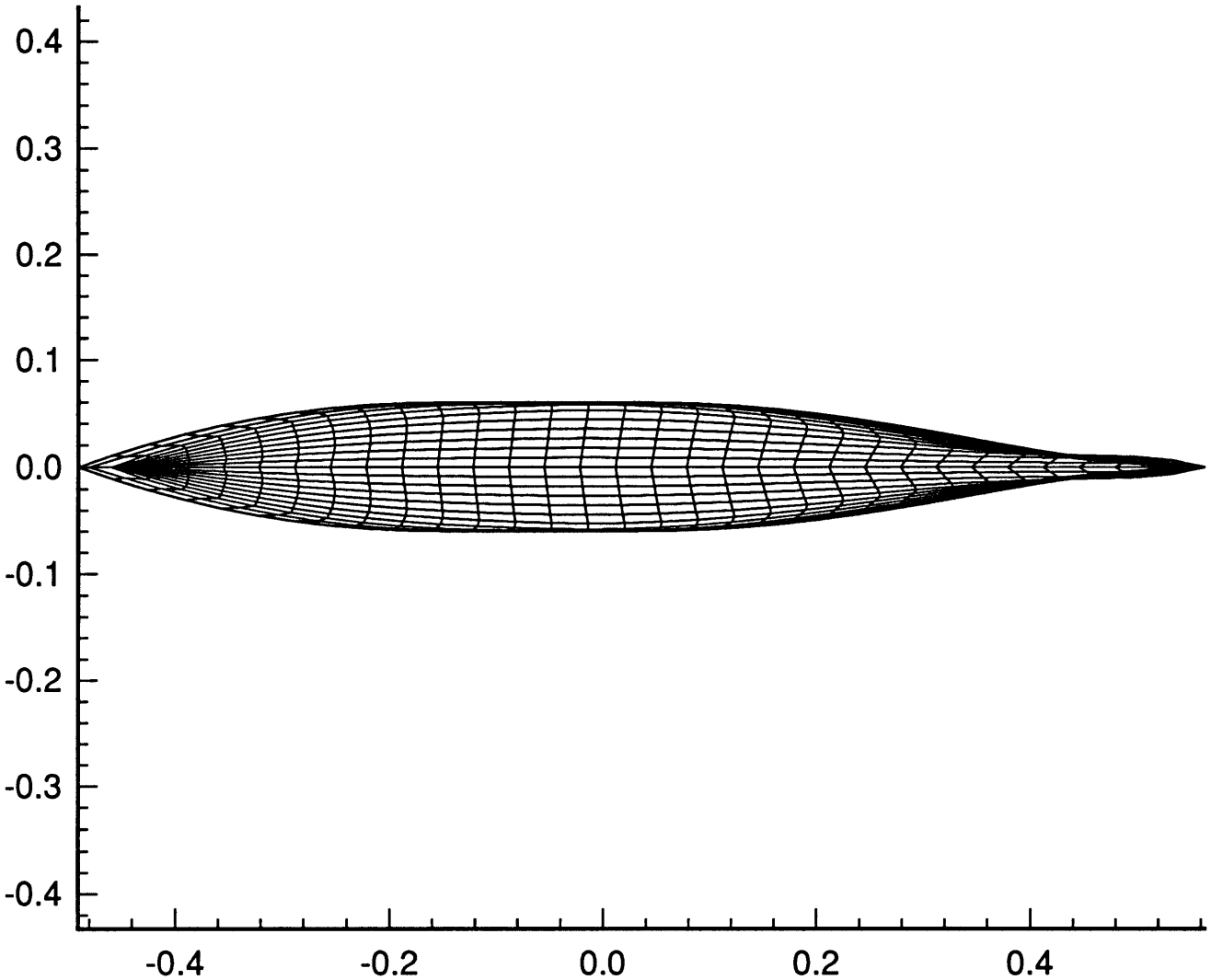

Figure 3: SL-7 hull Used in simulations—scaled to extreme size (L=300 meters)

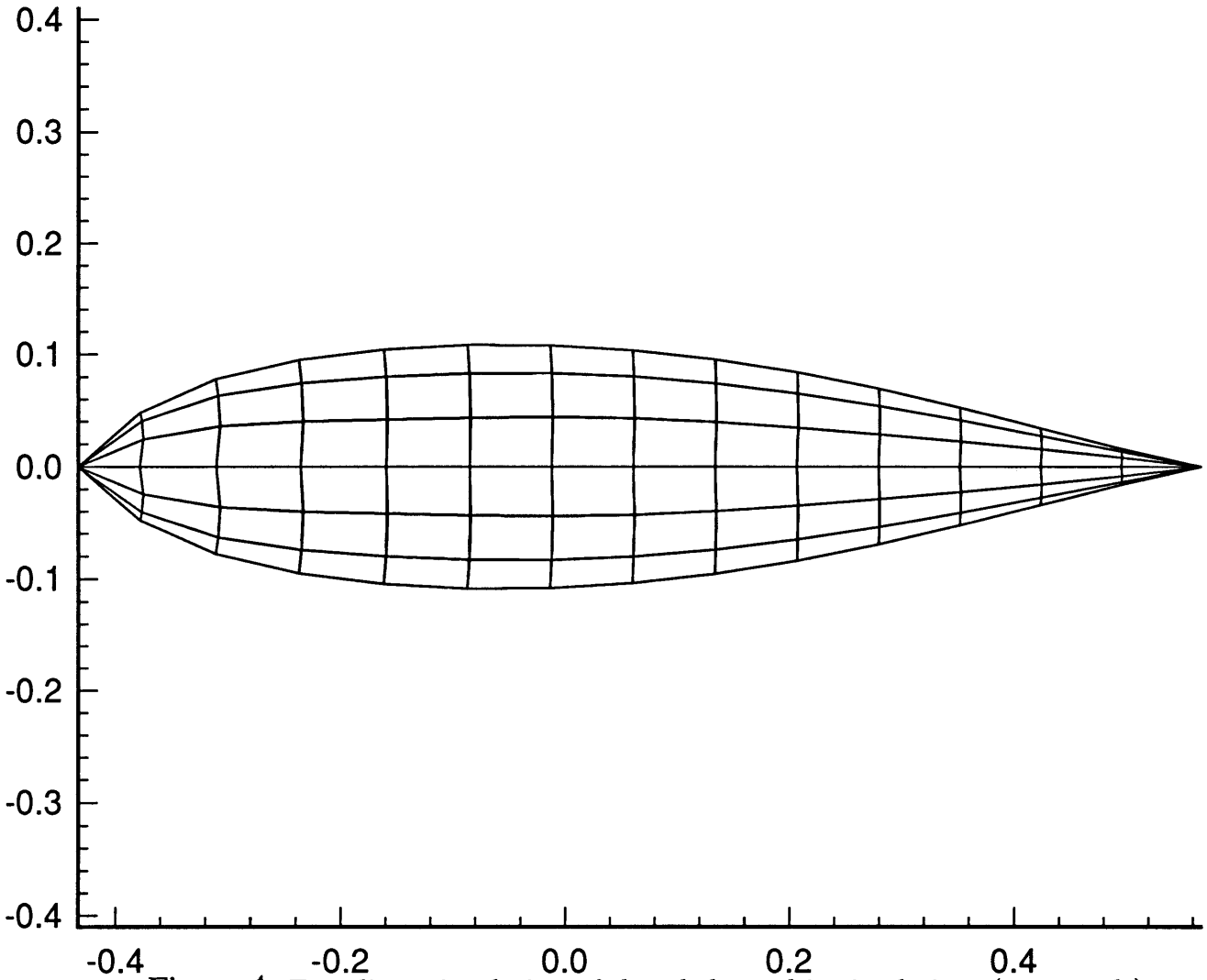

Figure 4: Two-dimensional view of the whale used in simulations (196 panels)

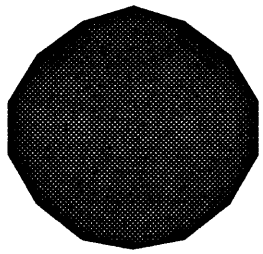

Figure 5: **Front view of the whale used in simulations (196 panels)**

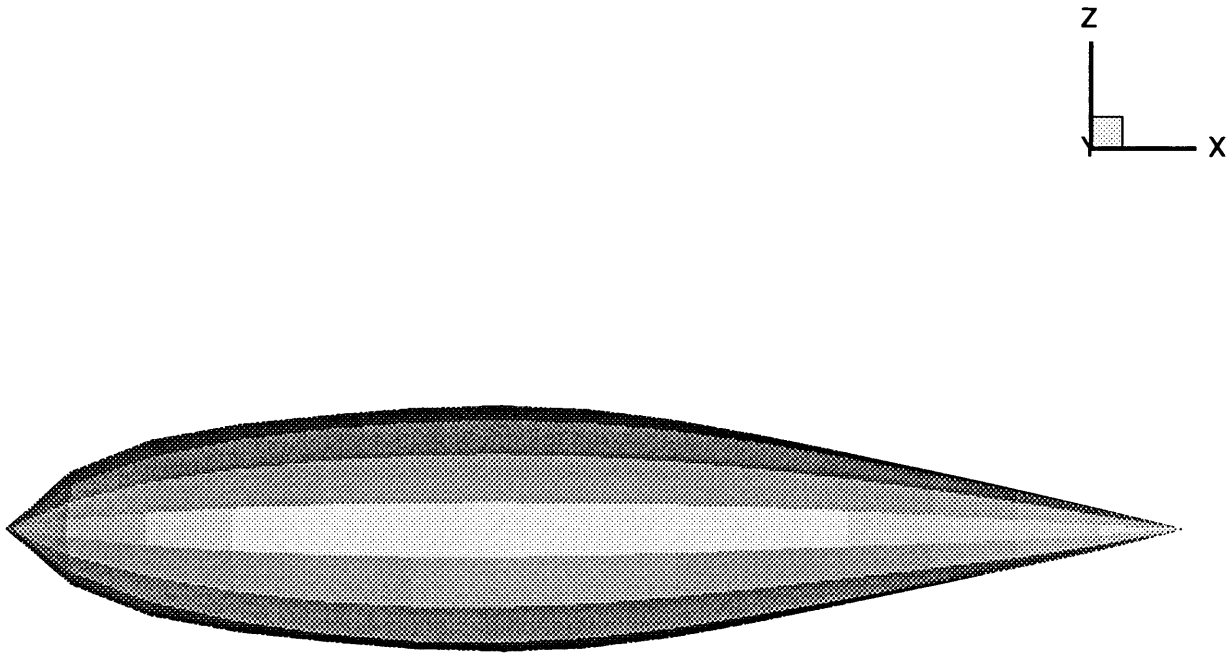

Figure 6: Side view of the whale used in simulations (196 panels)

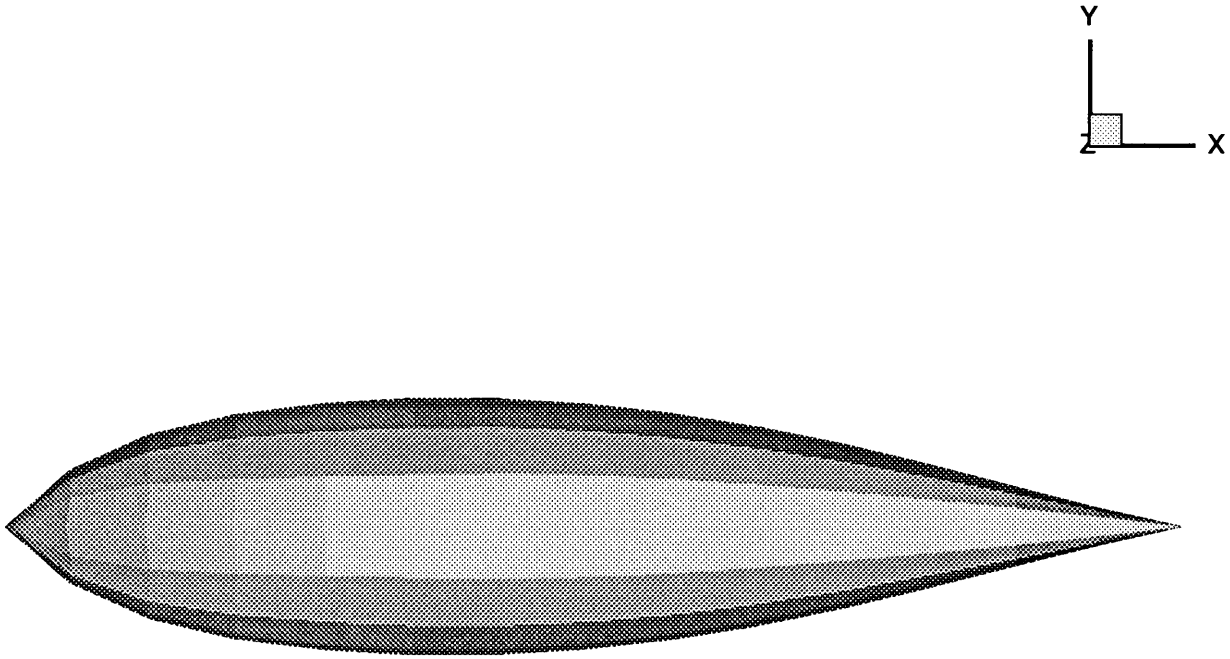

Figure 7: Top view of the whale used in simulations (196 panels)

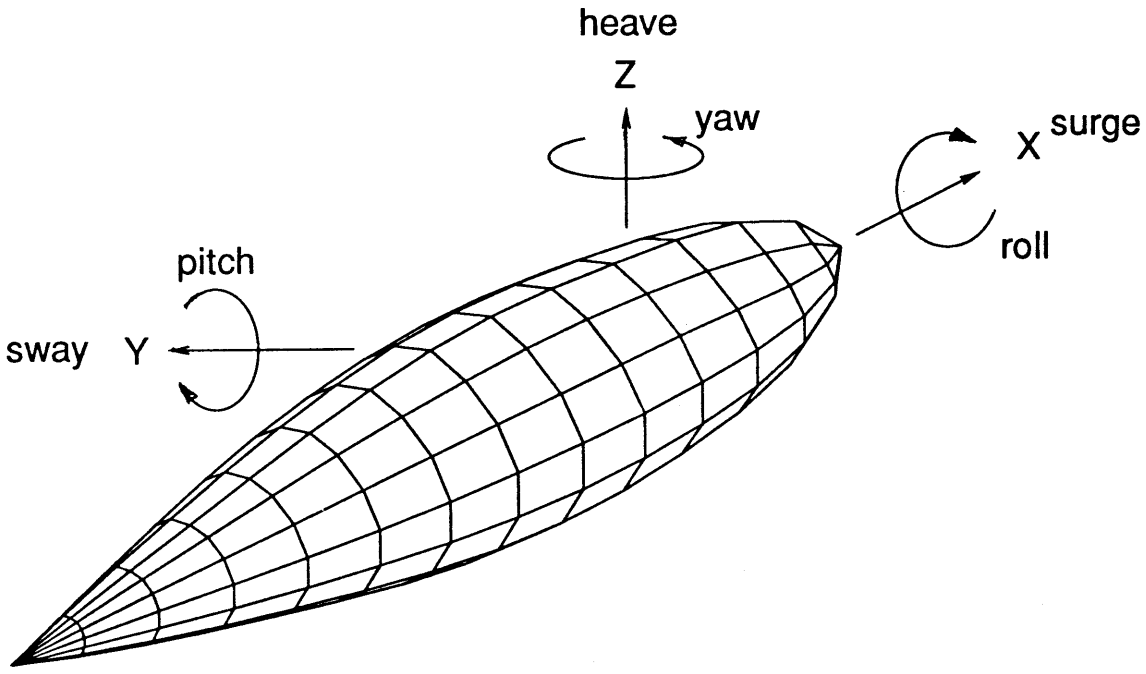

Figure 8: Direction of hydrodynamic forces imposed on a right whale

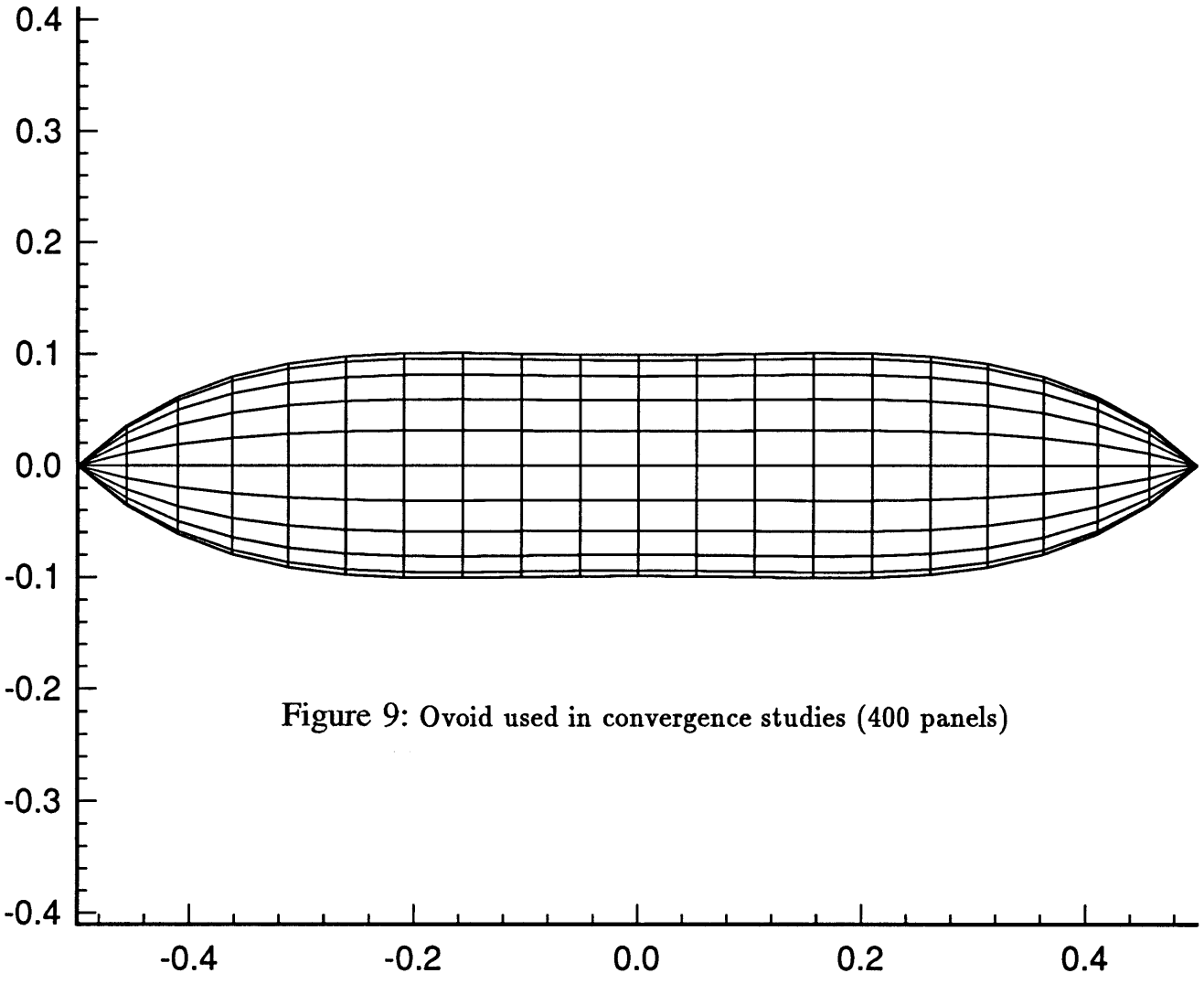

Figure 9: Ovoid used in convergence studies (400 panels)

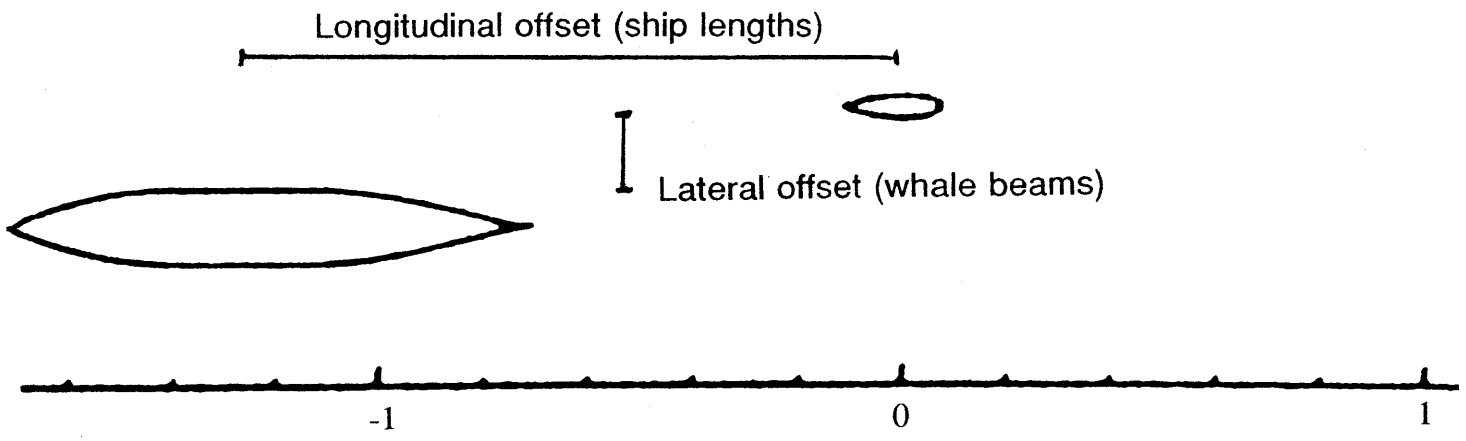

Figure 10: Depiction of lateral and longitudinal offsets

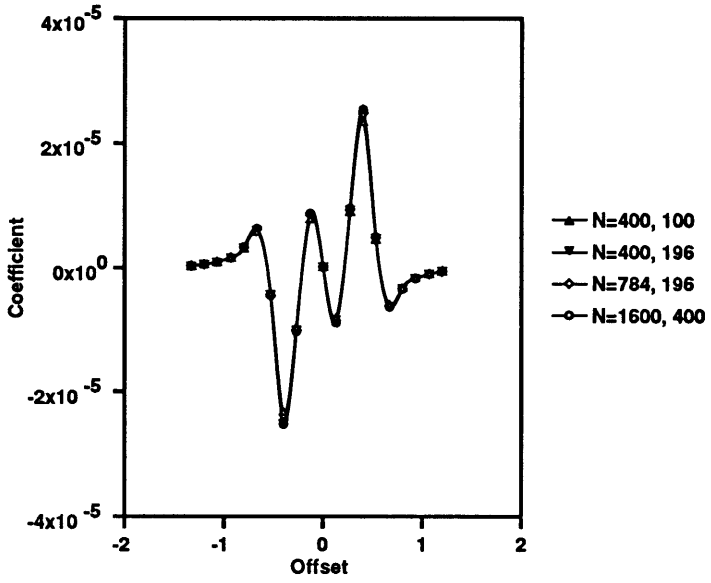

Figure 11: Surge coefficient for the whale for surface panel number convergence at 1 whale beam apart (3 meters) (N=number of panels ship, whale)

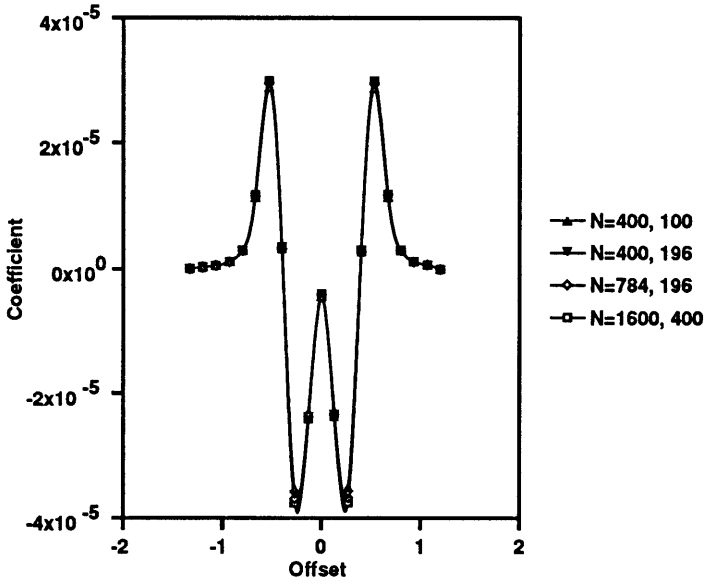

Figure 12: Sway coefficient for the whale for surface panel number convergence at 1 whale beam apart (3 meters) (N=number of panels ship, whale)

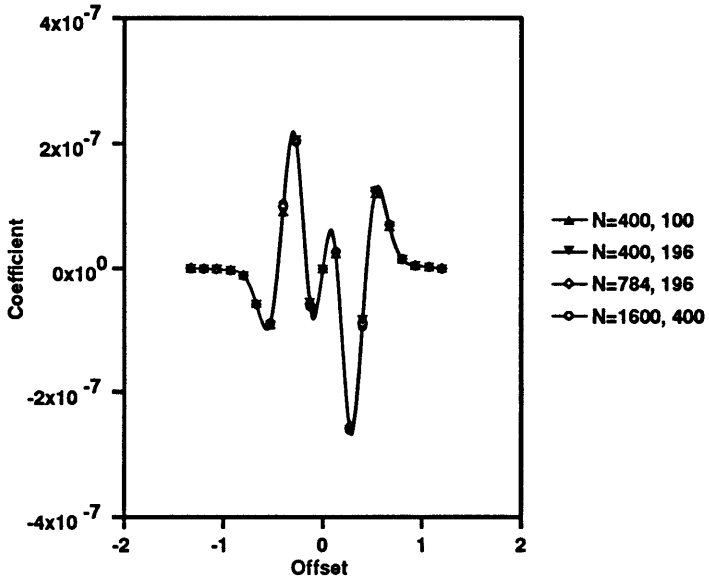

Figure 13: Yaw coefficient for the whale for surface panel number convergence at 1 whale beam apart (3 meters) (N=number of panels ship, whale)

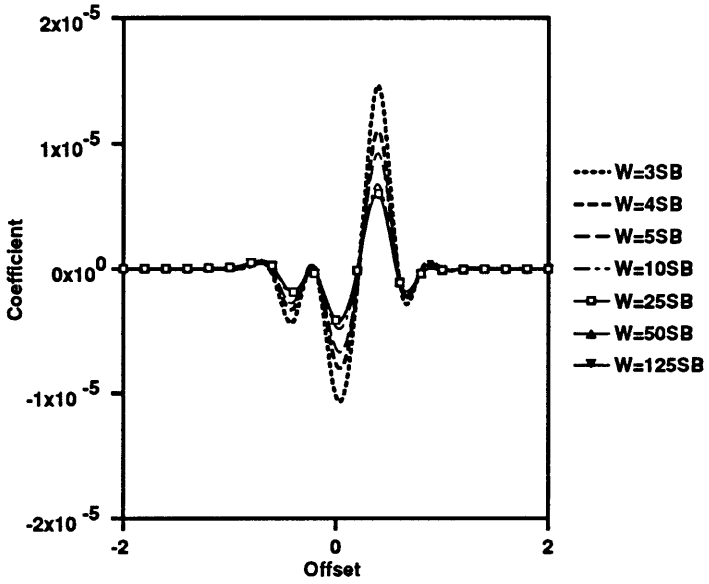

Figure 14: Surge coefficient for the whale for channel width convergence test for "infinite" width (SB=ship beam)

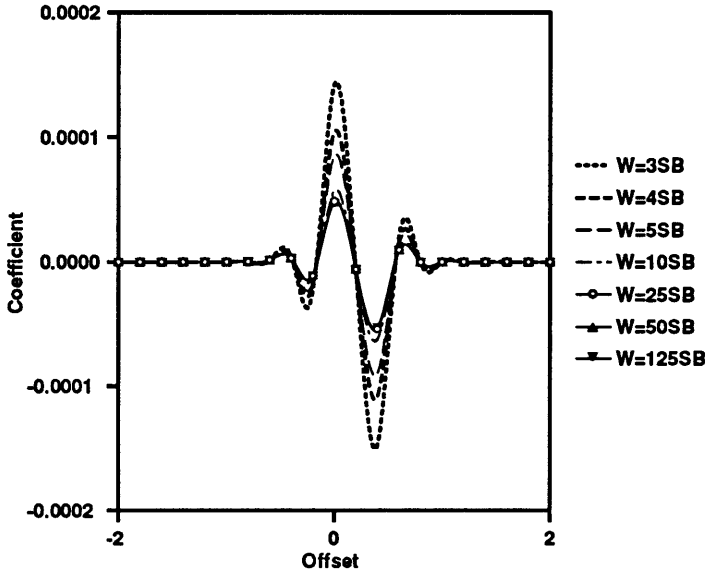

Figure 15: Sway coefficient for the whale for channel width convergence test for "infinite" width (SB=ship beam)

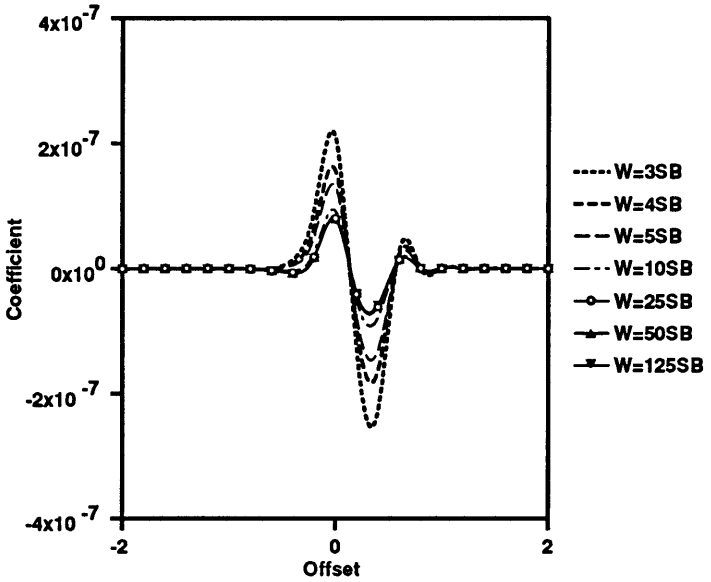

Figure 16: Yaw coefficient for the whale for channel width convergence test for "infinite" width (SB=ship beam)

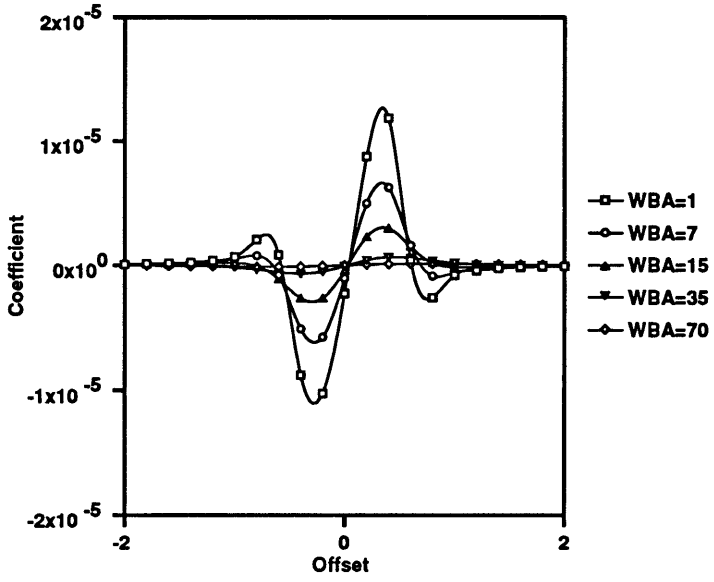

Figure 17: Surge coefficient for the whale for the Mariner and whale simulations at infinite channel width and 42ft channel depth for varying distances between the whale and the ship

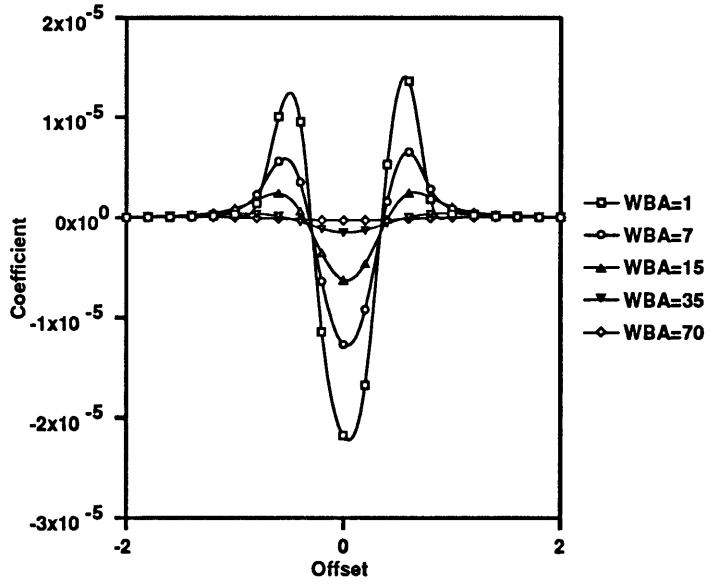

Figure 18: Sway coefficient for the whale for the Mariner and whale simulations at infinite channel width and 42ft channel depth for varying distances between the whale and the ship

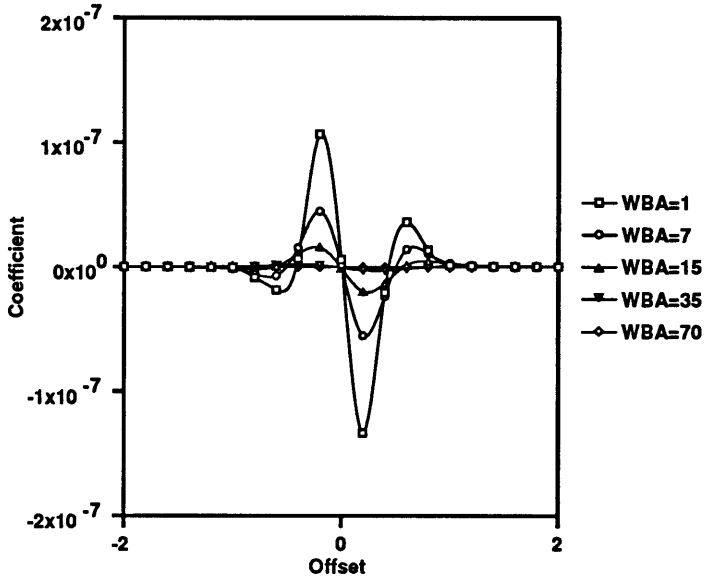

Figure 19: Yaw coefficient on the whale for the Mariner and whale simulations at infinite channel width and 42ft channel depth for varying distances between the whale and the ship

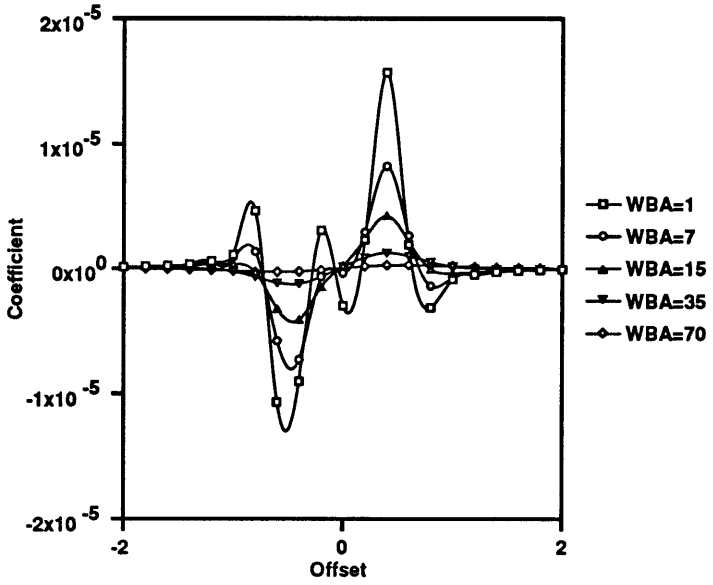

Figure 20: Surge coefficient on the whale for the Panamax and whale simulations at infinite channel width and 42ft channel depth for varying distances between the whale and the ship

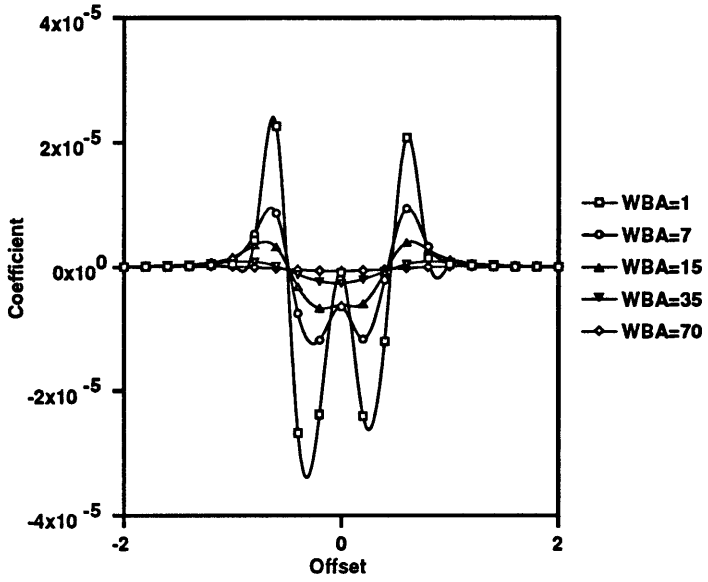

Figure 21: Sway coefficient on the whale for the Panamax and whale simulations at infinite channel width and 42ft channel depth for varying distances between the whale and the ship

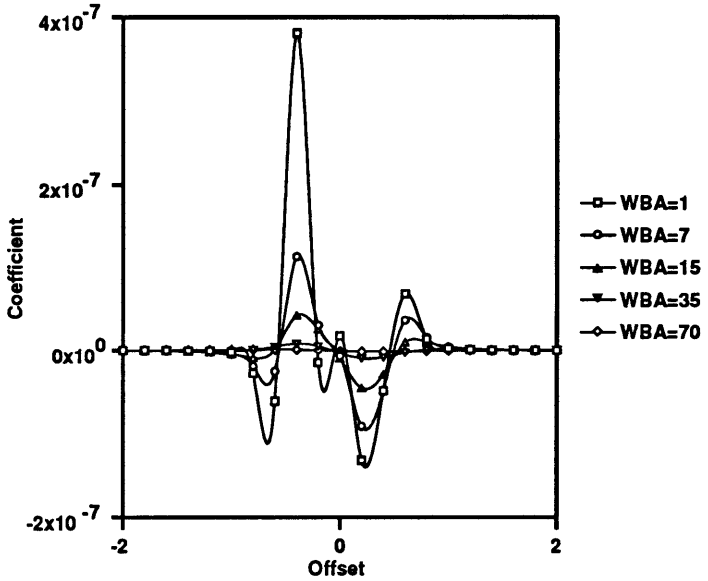

Figure 22: Yaw coefficient on the whale for the Panamax and whale simulations at infinite channel width and 42ft channel depth for varying distances between the whale and the ship

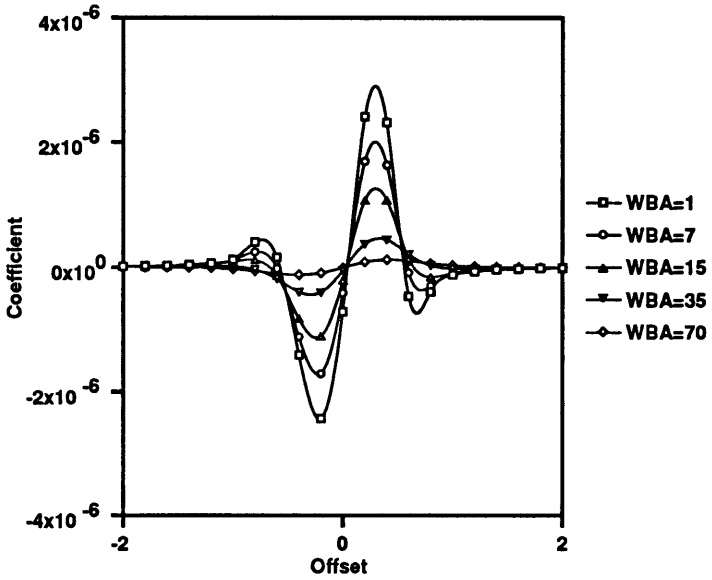

Figure 23: Surge coefficient on the whale for the SL-7 and whale simulations at infinite channel width and 42ft channel depth for varying distances between the whale and the ship

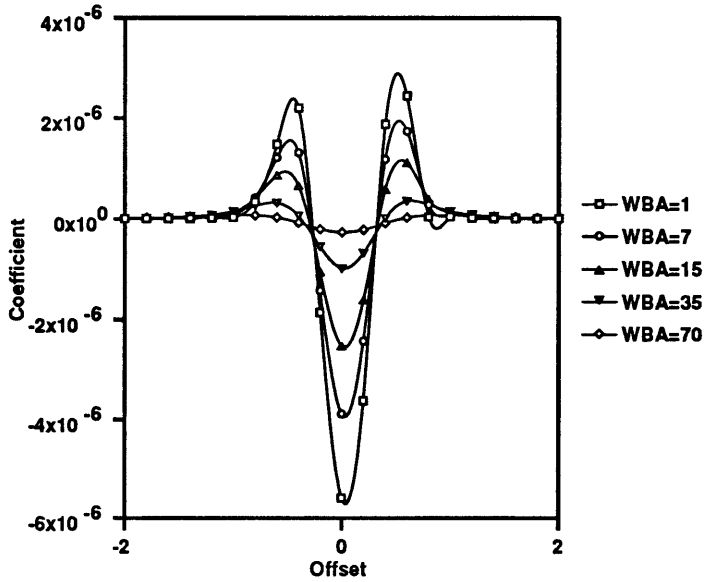

Figure 24: Sway coefficient on the whale for the SL-7 and whale simulations at infinite channel width and 42ft channel depth for varying distances between the whale and the ship

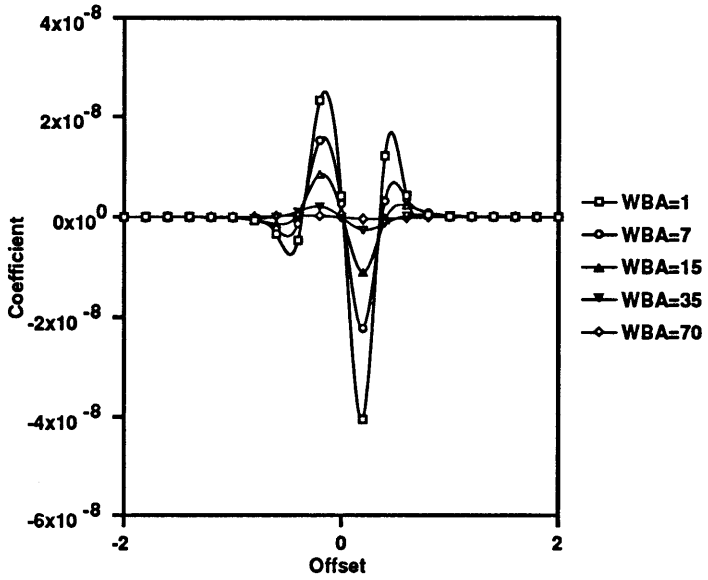

Figure 25: Yaw coefficient on the whale for the SL-7 and whale simulations at infinite channel width and 42ft channel depth for varying distances between the whale and the ship

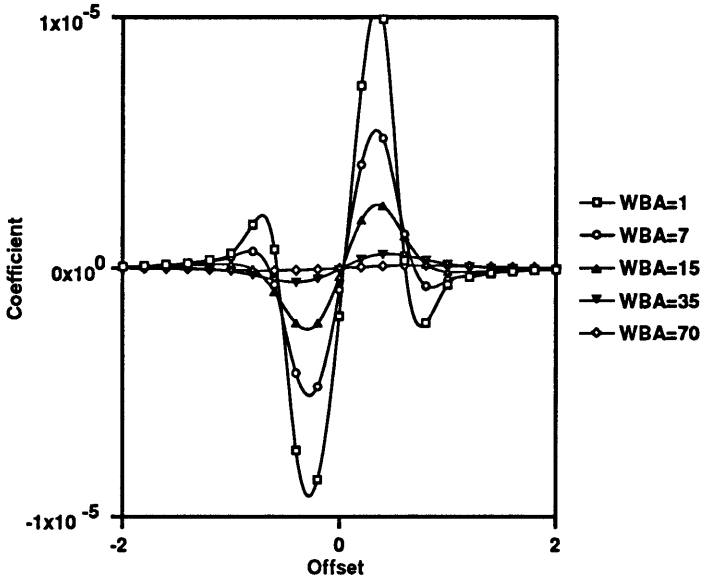

Figure 26: surge coefficient on the whale for the Mariner and whale simulations at infinite channel width and 50ft channel depth for varying distances between the whale and the ship

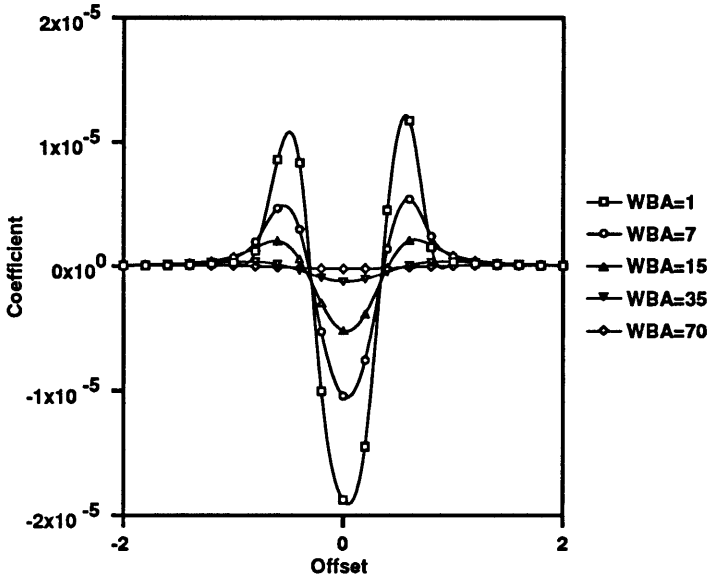

Figure 27: Sway coefficient on the whale for the Mariner and whale simulations at infinite channel width and 50ft channel depth for varying distances between the whale and the ship

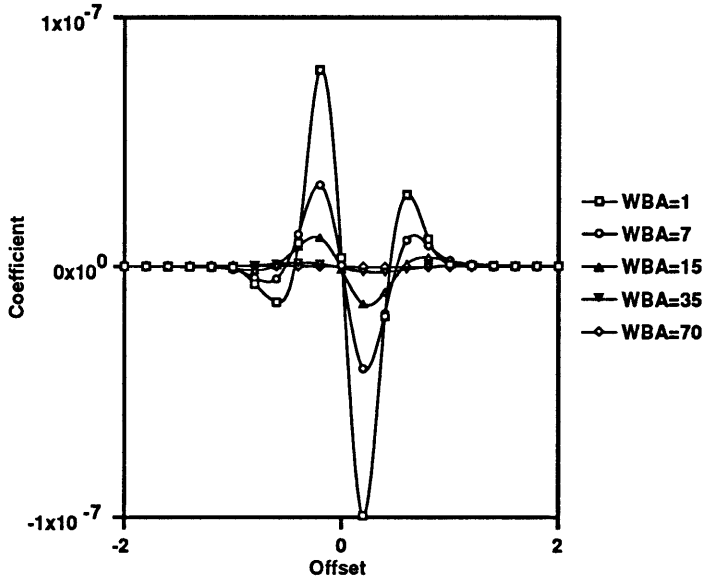

Figure 28: Yaw coefficient on the whale for the Mariner and whale simulations at infinite channel width and 50ft channel depth for varying distances between the whale and the ship

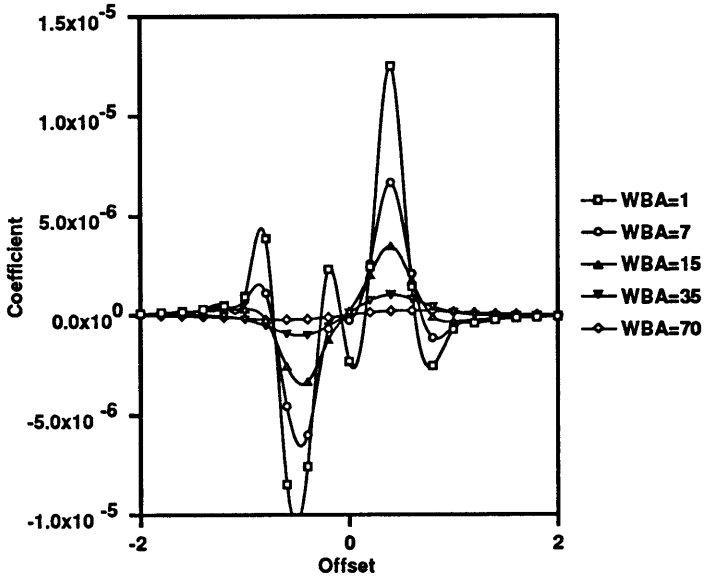

Figure 29: Surge coefficient on the whale for the Panamax and whale simulations at infinite channel width and 50ft channel depth for varying distances between the whale and the ship

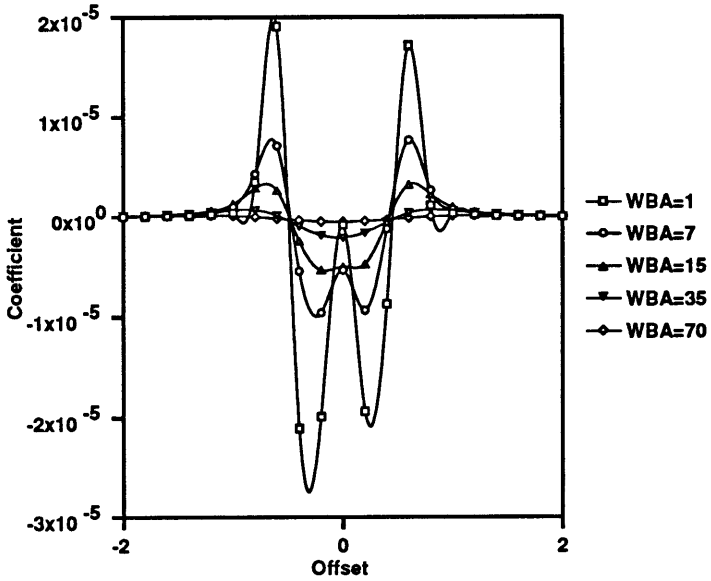

Figure 30: Sway coefficient on the whale for the Panamax and whale simulations at infinite channel width and 50ft channel depth for varying distances between the whale and the ship

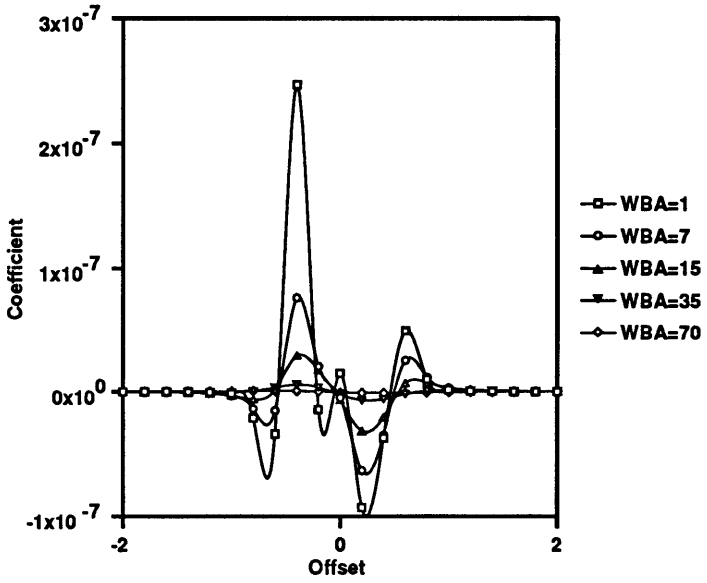

Figure 31: yaw coefficient on the whale for the Panamax and whale simulations at infinite channel width and 50ft channel depth for varying distances between the whale and the ship

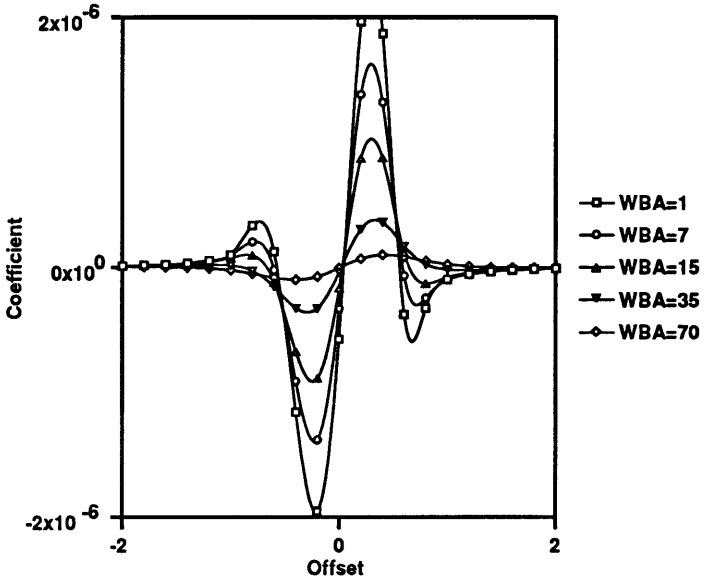

Figure 32: Surge coefficient on the whale for the SL-7 and whale simulations at infinite channel width and 50ft channel depth for varying distances between the whale and the ship

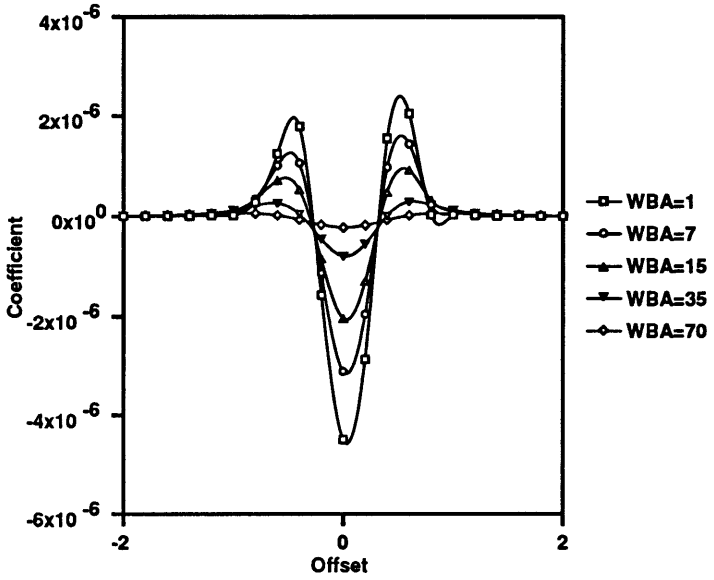

Figure 33: Sway coefficient on the whale for the SL-7 and whale simulations at infinite channel width and 50ft channel depth for varying distances between the whale and the ship

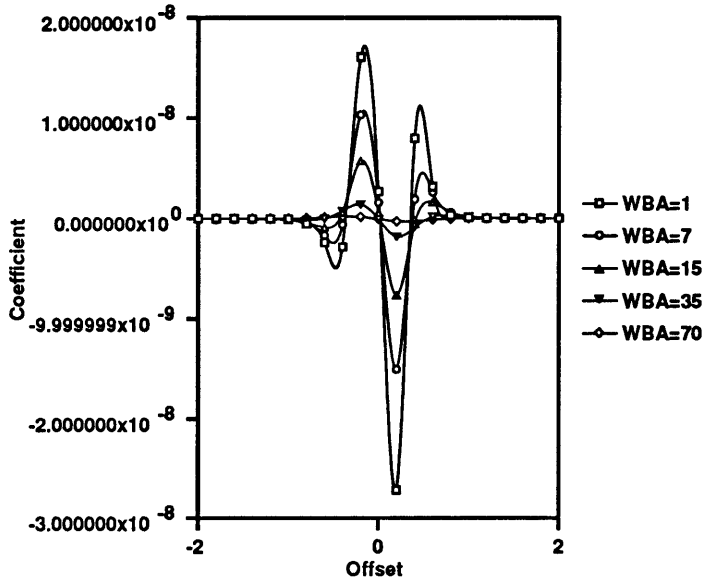

Figure 34: Yaw coefficient on the whale for the SL-7 and whale simulations at infinite channel width and 50ft channel depth for varying distances between the whale and the ship

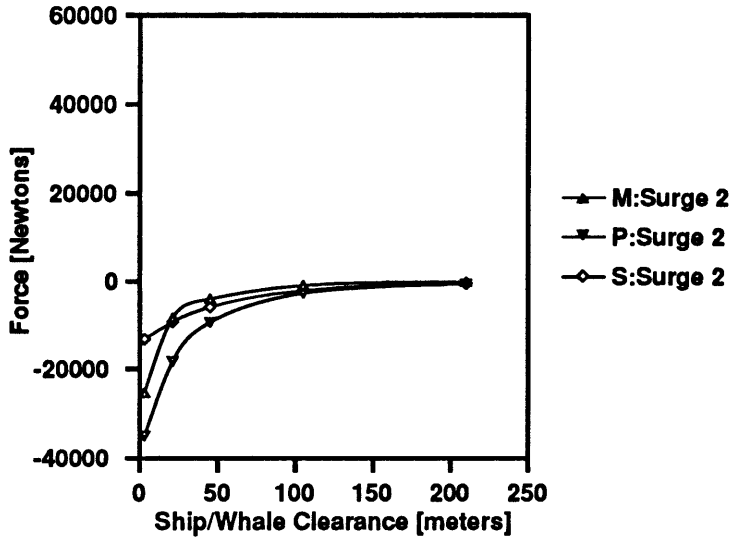

Figure 35: Maximum surge force for the whale in a channel of infinite width and 42ft depth (M=Mariner; P=Panamax; S=SL-7)

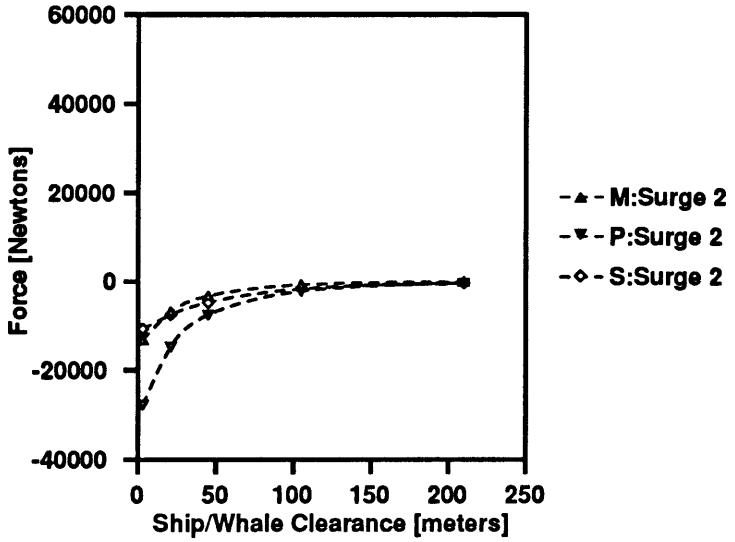

Figure 36: Maximum surge force for the whale in a channel of infinite width and 50ft depth (M=Mariner; P=Panamax; S=SL-7)

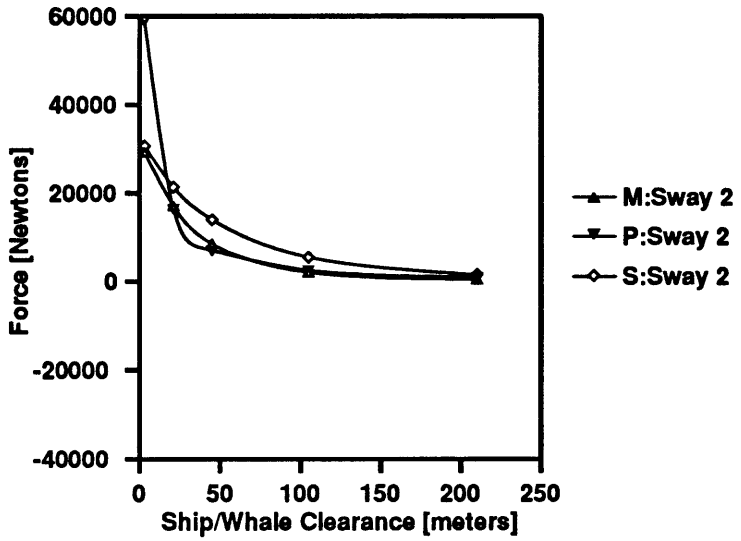

Figure 37: Maximum sway force for the whale in a channel of infinite width and 42ft depth (M=Mariner; P=Panamax; S=SL-7)

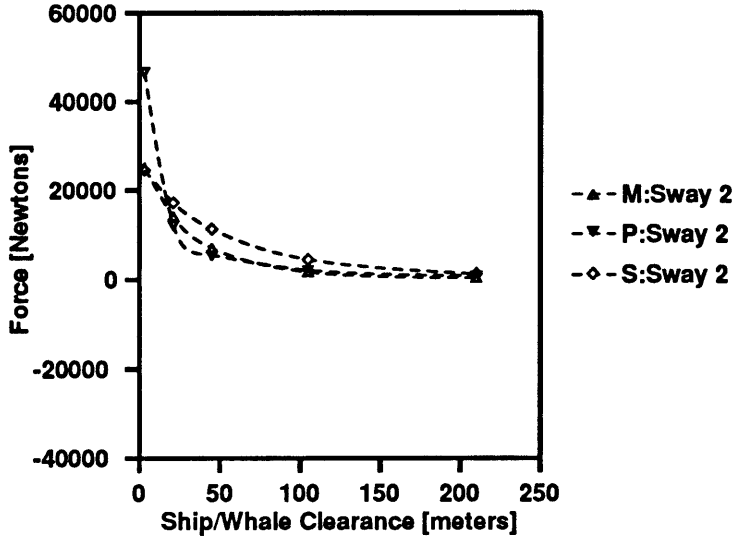

Figure 38: Maximum sway force for the whale in a channel of infinite width and 50ft depth (M=Mariner; P=Panamax; S=SL-7)

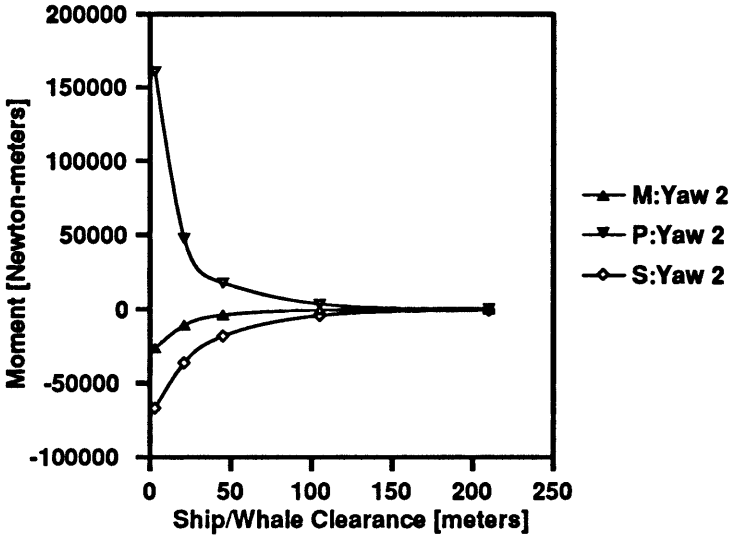

Figure 39: Maximum yaw momentfor the whale in a channel of infinite width and 42ft depth (M=Mariner; P=Panamax; S=SL-7)

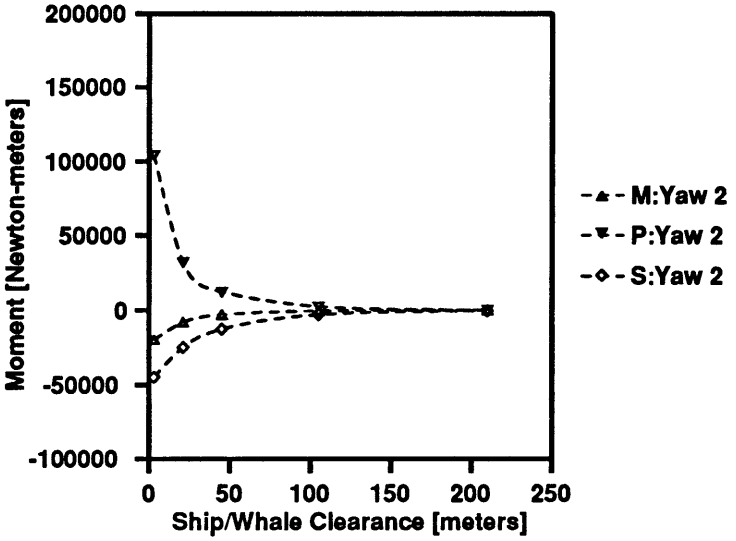

Figure 40: Maximum yaw moment for the whale in a channel of infinite width and 50ft depth (M=Mariner; P=Panamax; S=SL-7)

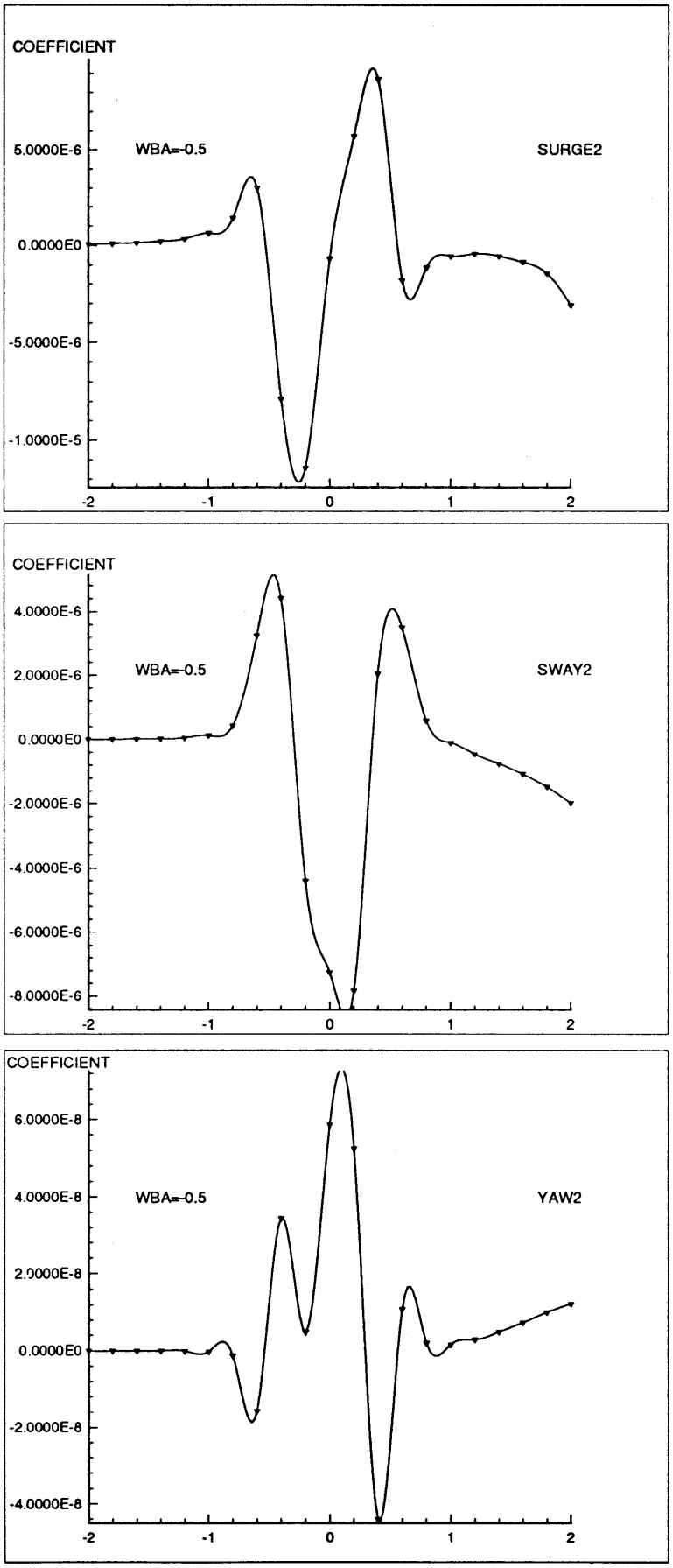

Figure 41: Force coefficients for the whale, for the Mariner and whale simulation at 42ft channel depth, whale initially at -0.5 whale beams from the side of the ship.

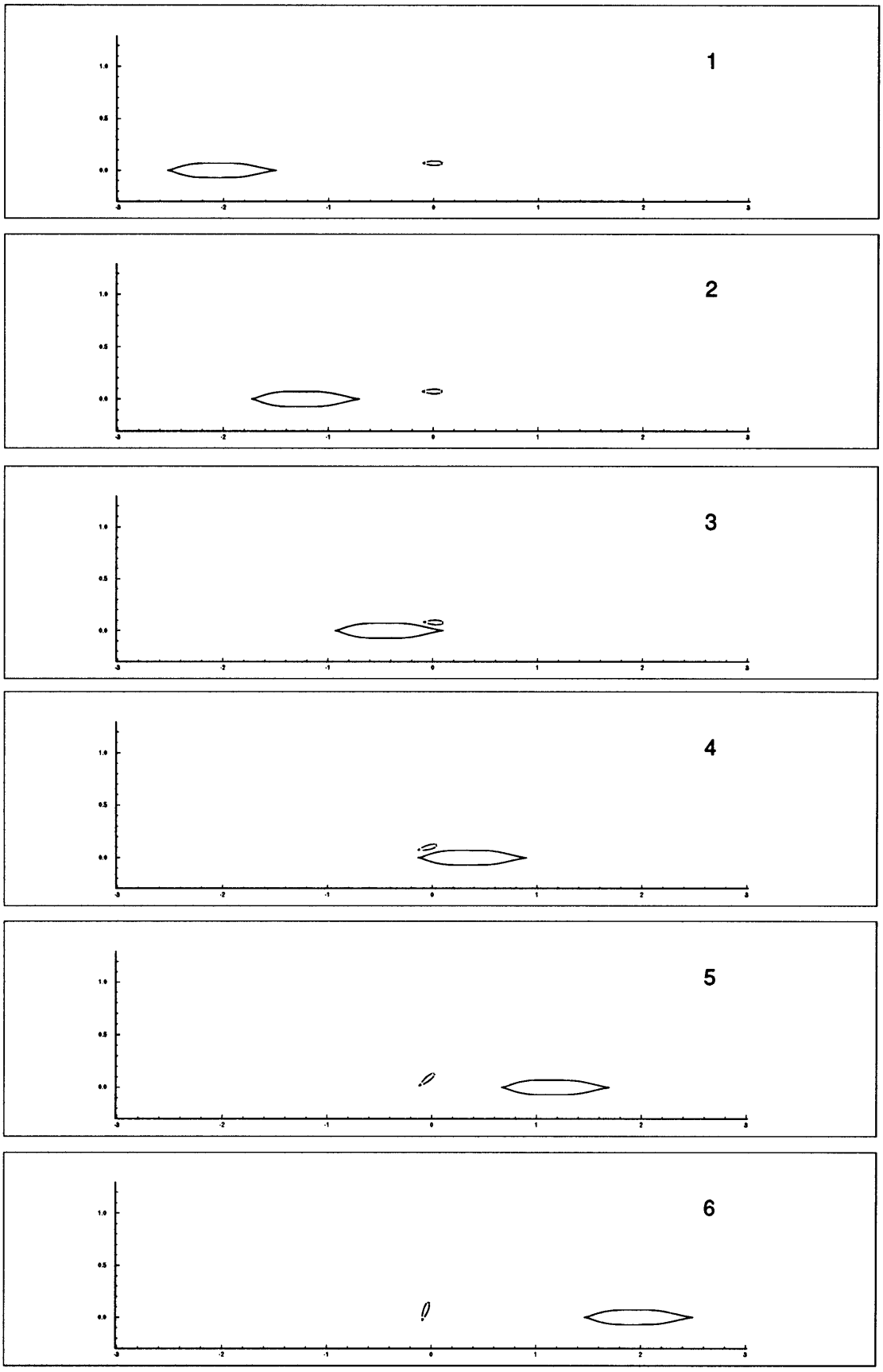

Figure 42: Positions of the whale and ship, for the Mariner and whale simulation at 42ft channel depth, whale initially at -0.5 whale beams from the side of the ship.

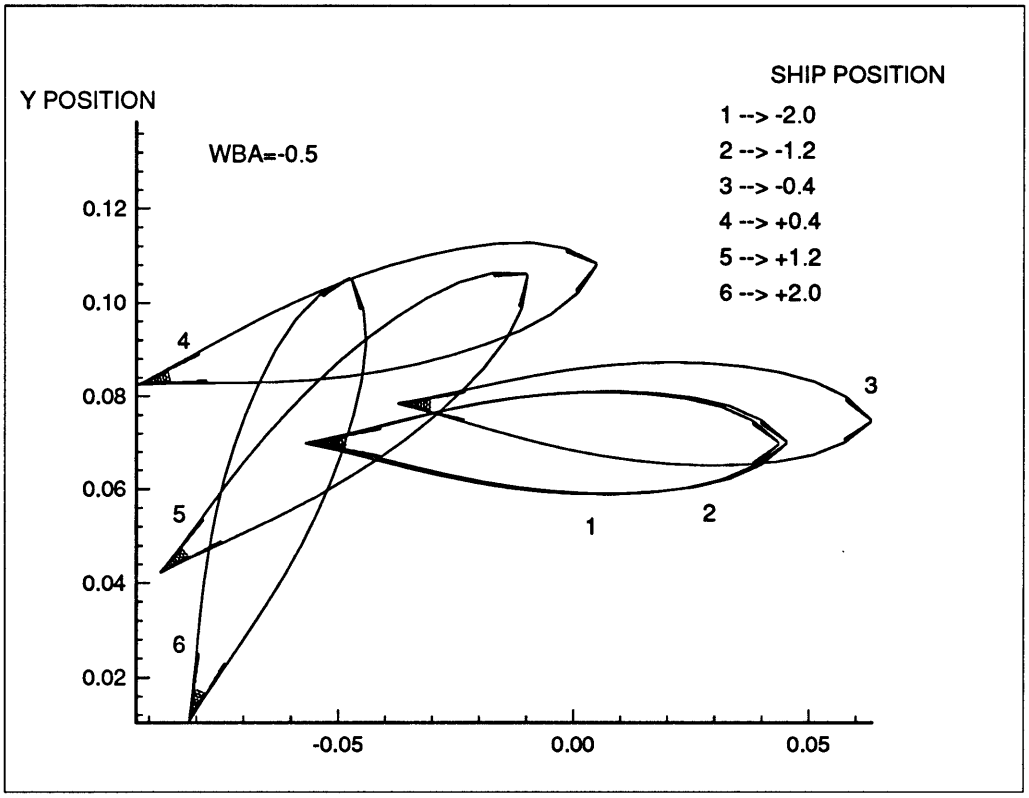

Figure 43: Positions of the whale, for the Mariner and whale simulation at 42ft channel depth, whale initially at -0.5 whale beams from the side of the ship.

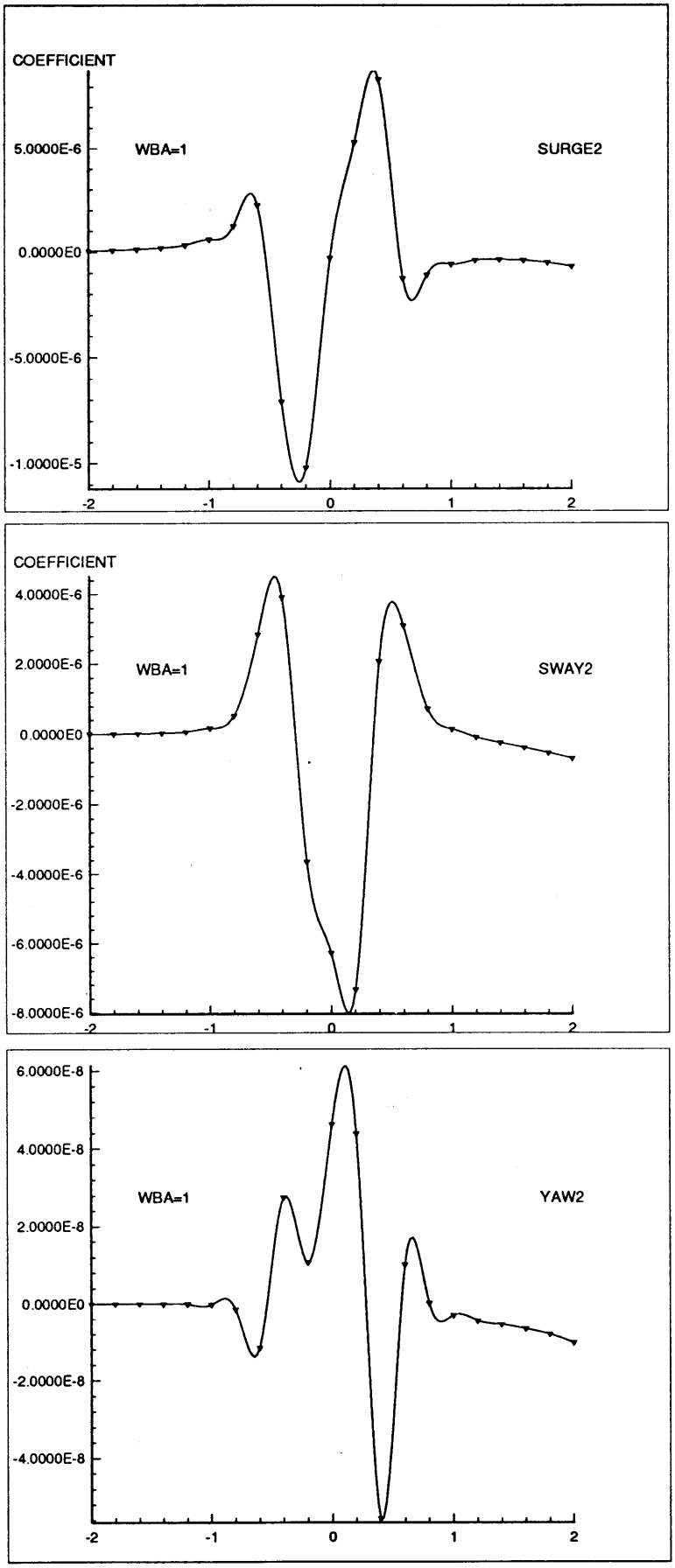

Figure 44: Force coefficients for the whale, for the Mariner and whale simulation at 42ft channel depth, whale initially at 1.0 whale beams from the side of the ship.

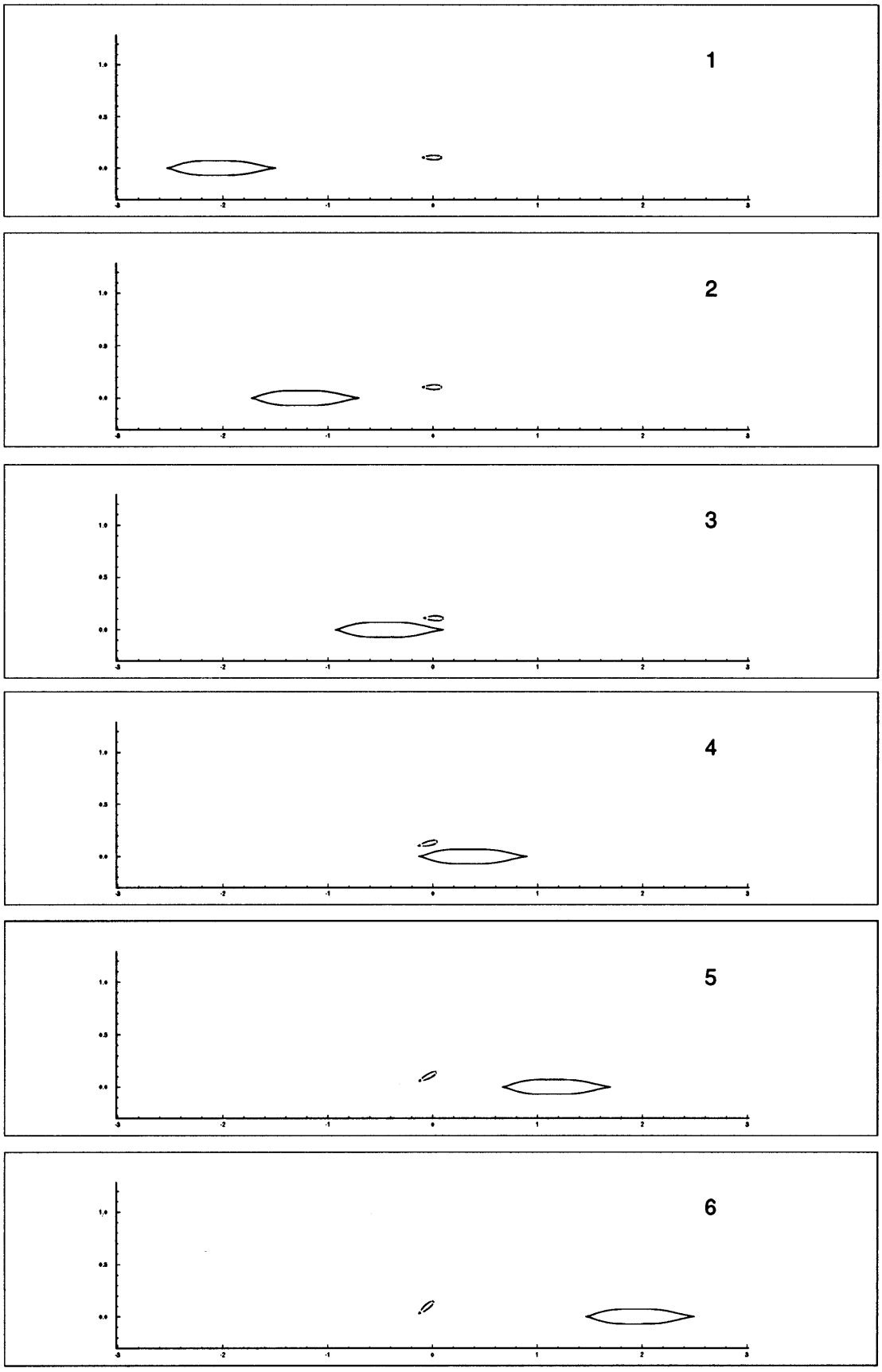

Figure 45: Positions of the whale and ship, for the Mariner and whale simulation at 42ft channel depth, whale initially at 1.0 whale beams from the side of the ship.

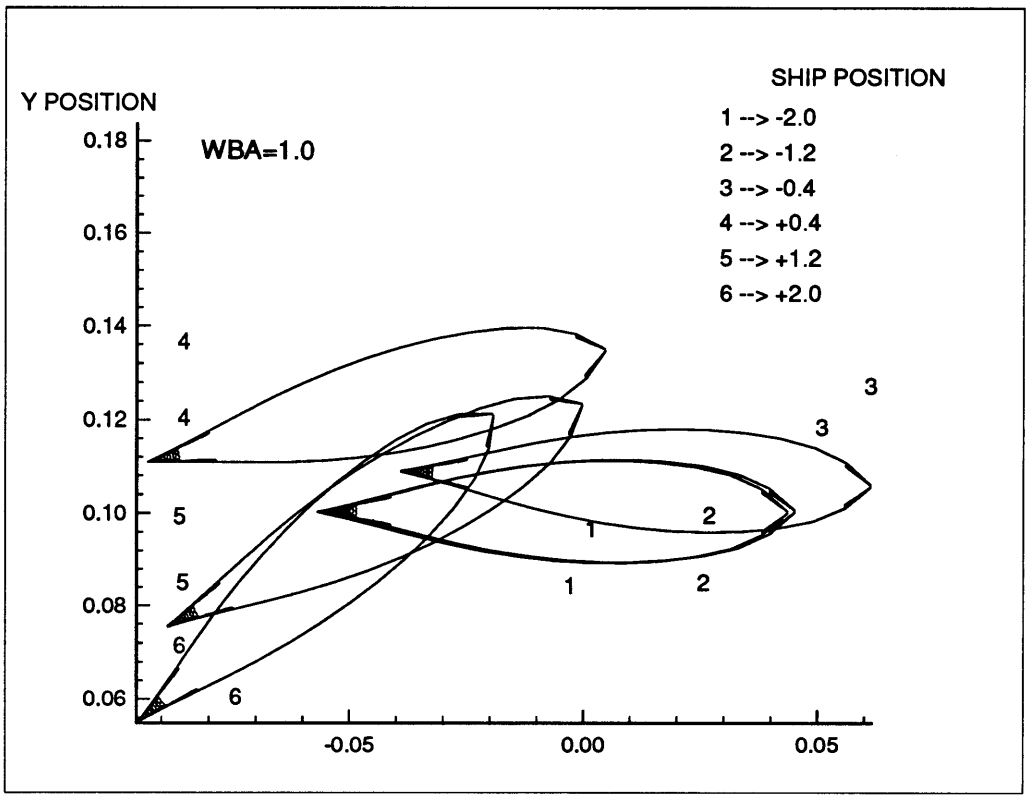

Figure 46: Positions of the whale, for the Mariner and whale simulation at 42ft channel depth, whale initially at 1.0 whale beams from the side of the ship.

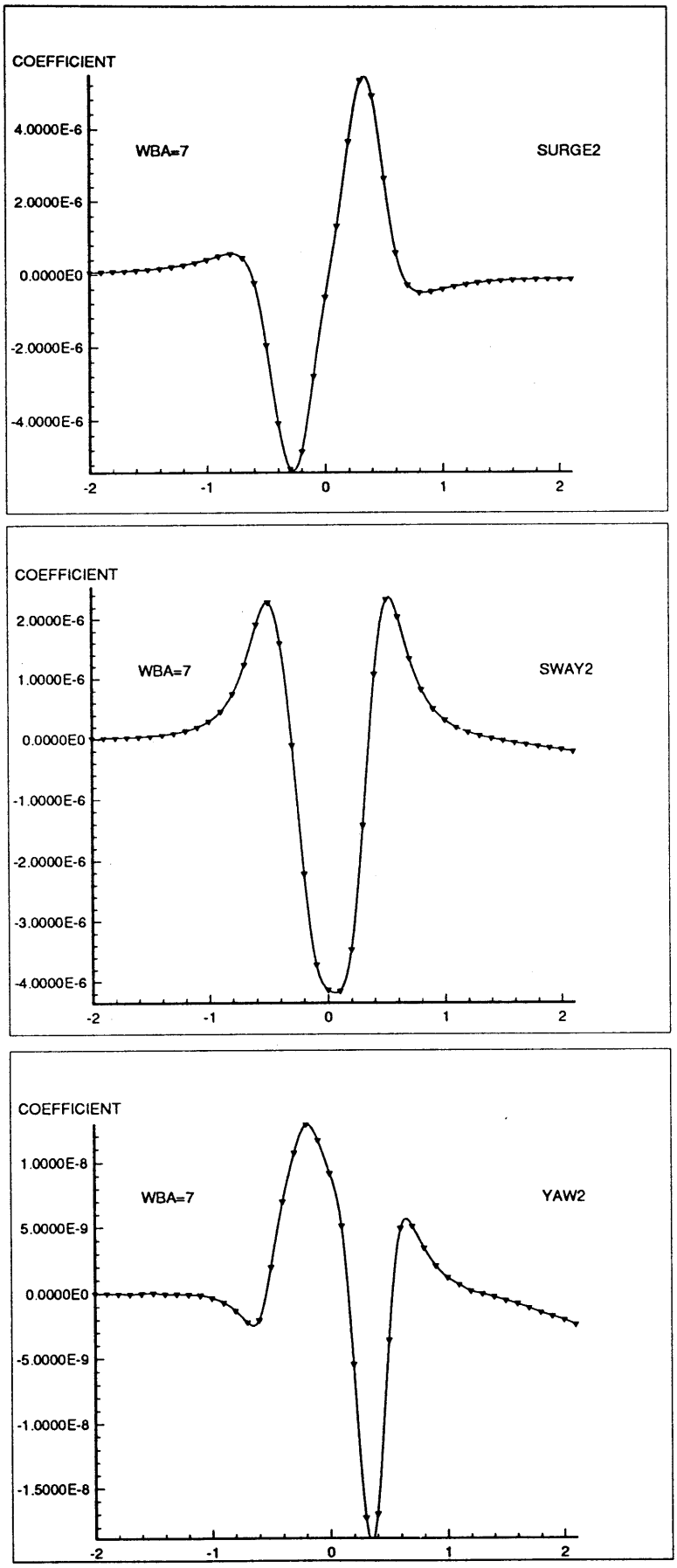

Figure 47: Force coefficients for the whale, for the Mariner and whale simulation at 42ft channel depth, whale initially at 7.0 whale beams from the side of the ship.

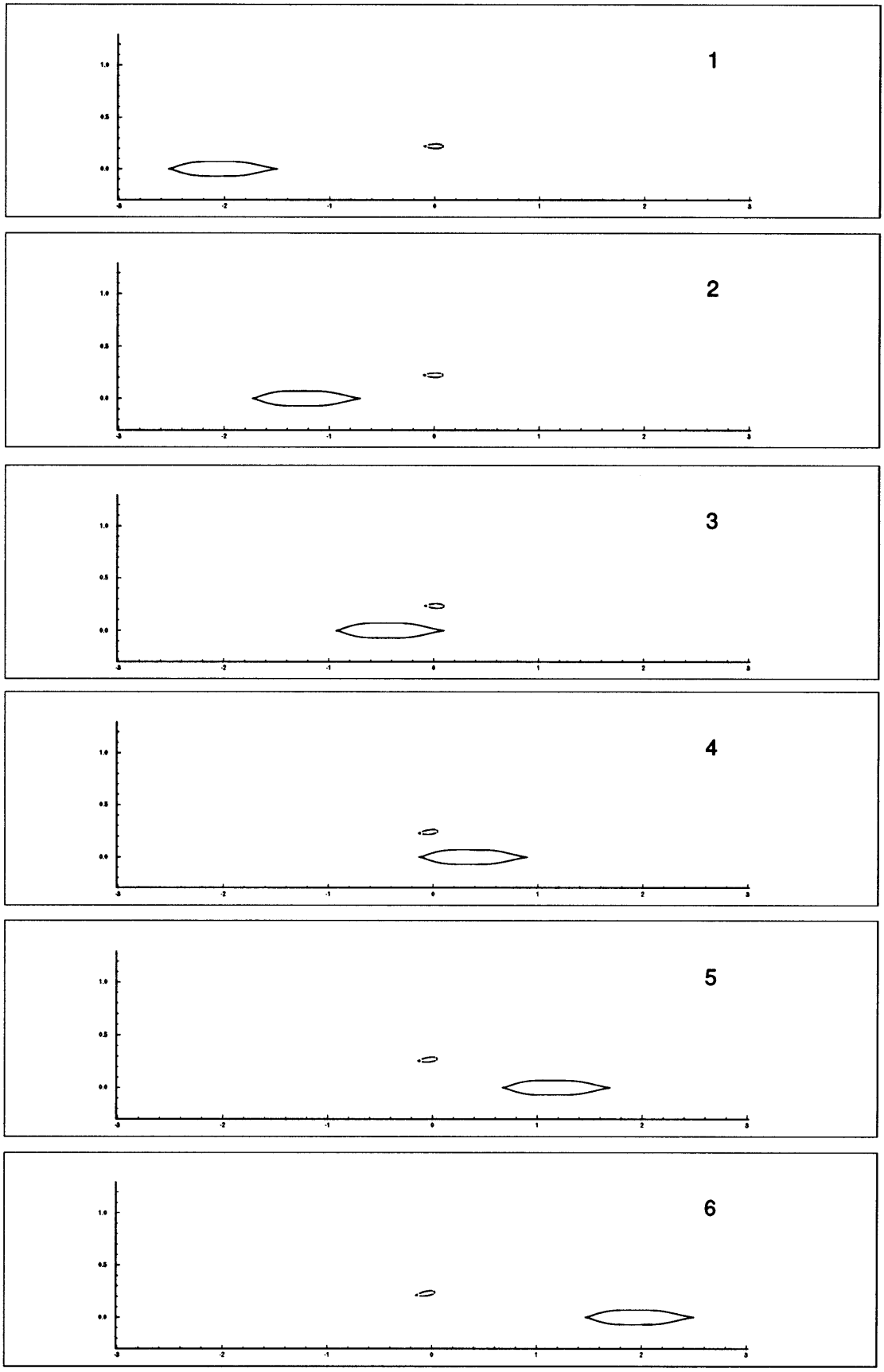

Figure 48: Positions of the whale and ship, for the Mariner and whale simulation at 42ft channel depth, whale initially at 7.0 whale beams from the side of the ship.

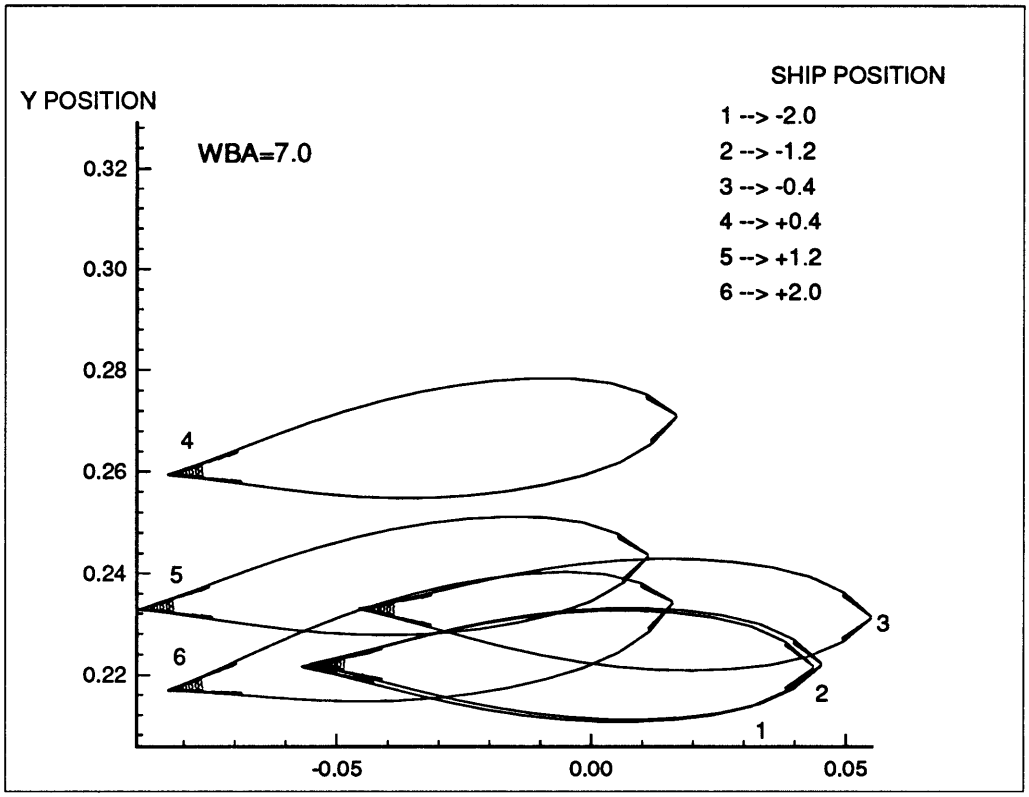

Figure 49: Positions of the whale, for the Mariner and whale simulation at 42ft channel depth, whale initially at 7.0 whale beams from the side of the ship.

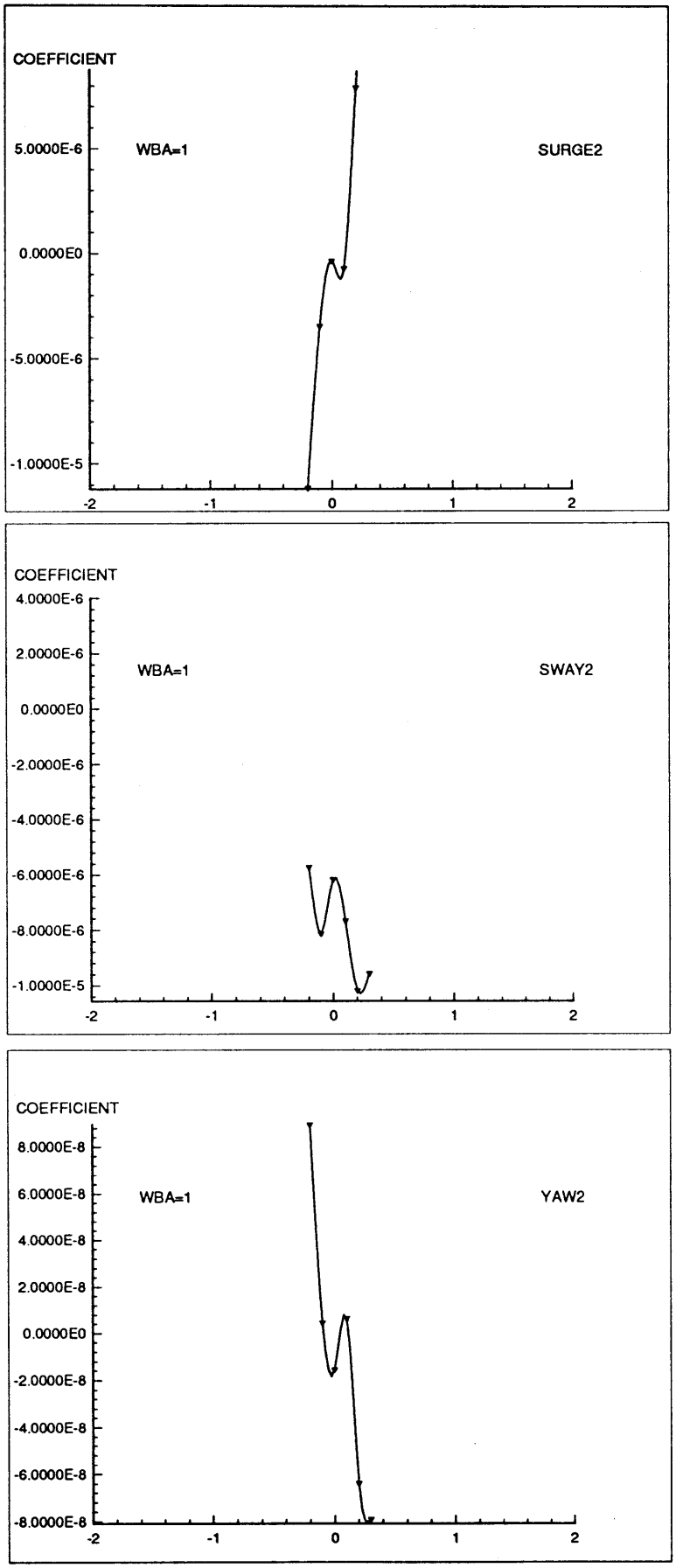

Figure 50: Force coefficients for the whale, for the Mariner and whale simulation at 42ft channel depth, whale "appears" at 1.0 whale beams from the side ofthe ship.

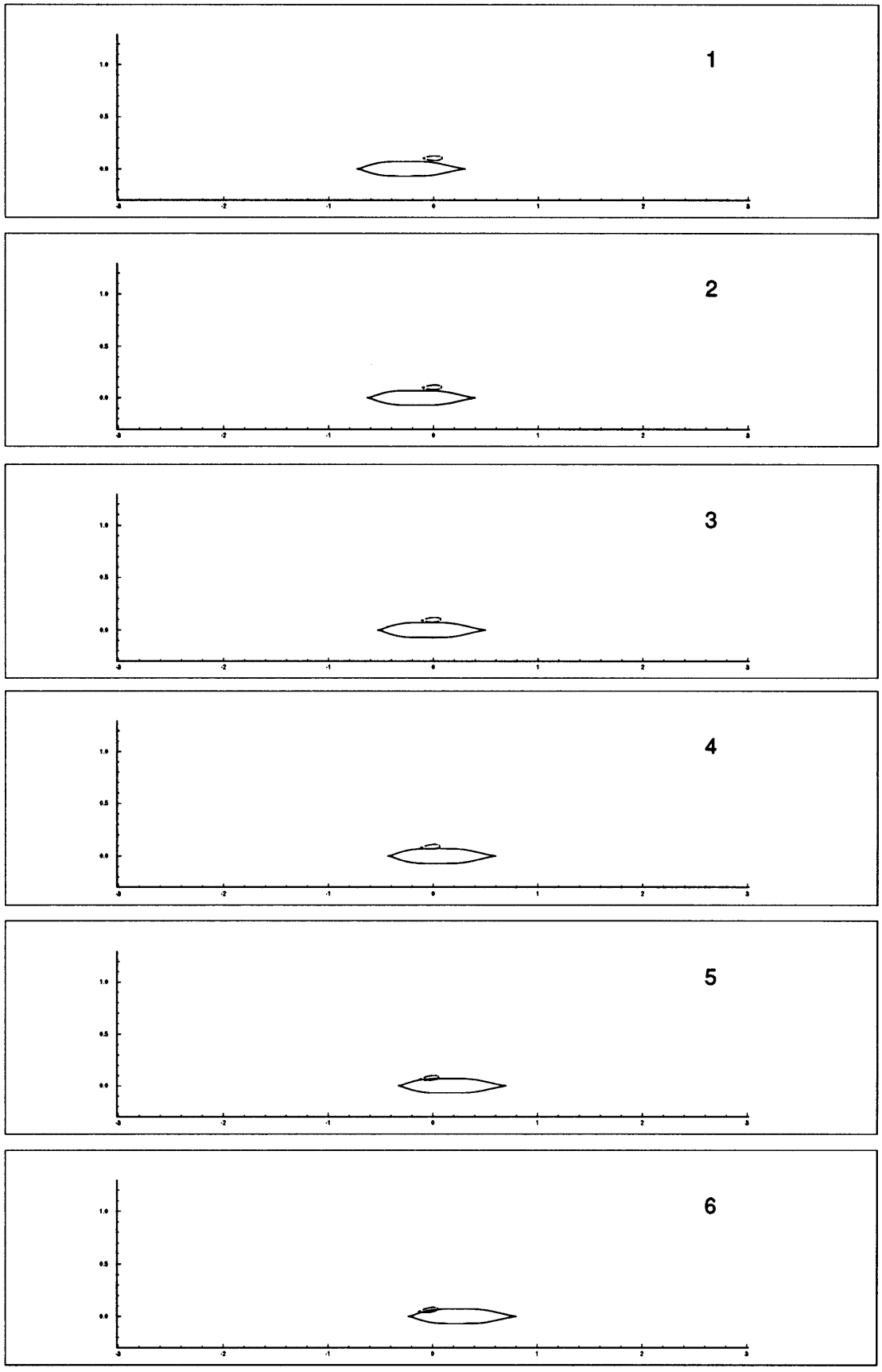

Figure 51: Positions of the whale and ship, for the Mariner and whale simulation at 42ft channel depth, whale "appears" at 1.0 whale beams from the side of the ship.

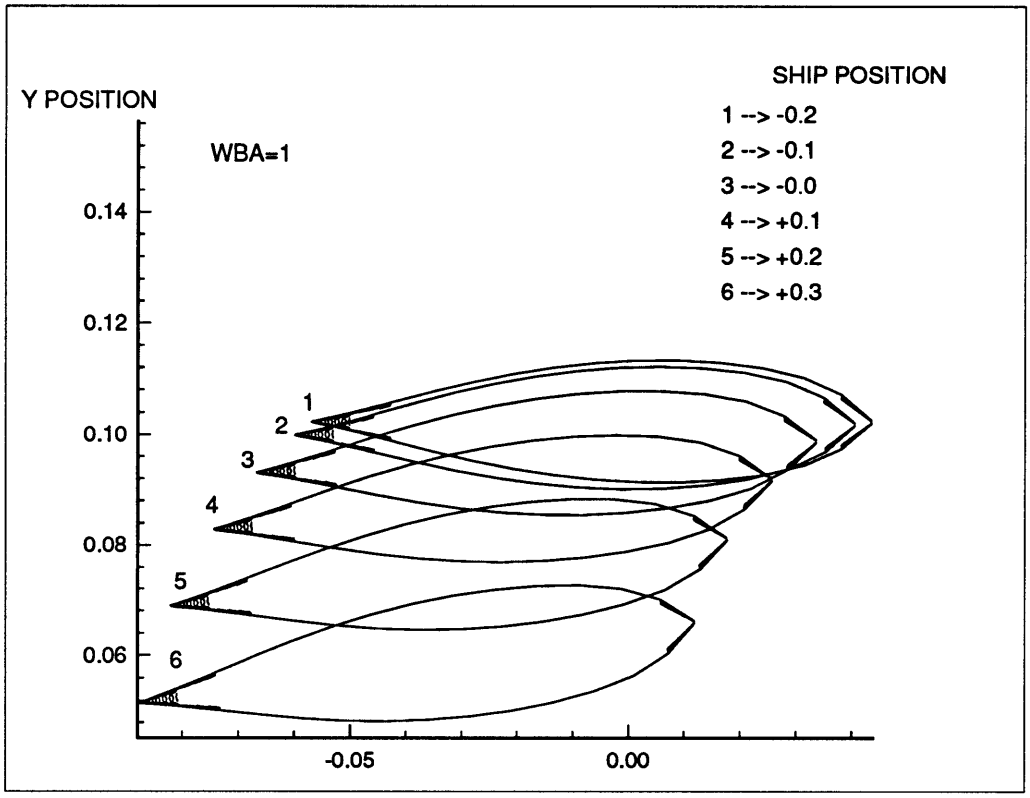

Figure 52: Positions of the whale, for the Mariner and whale simulation at 42ft channel depth, whale "appears" at 1.0 whale beams from the side of the ship.

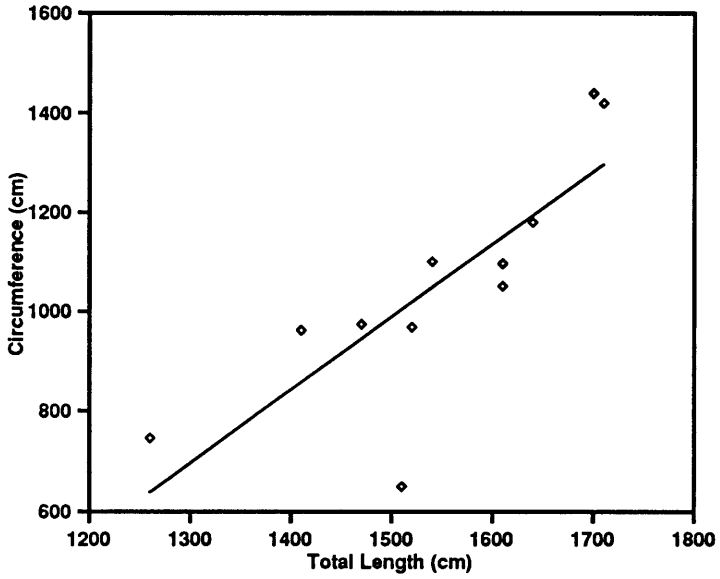

Figure 53: Linear least square fit plot of circumference at front of flipper

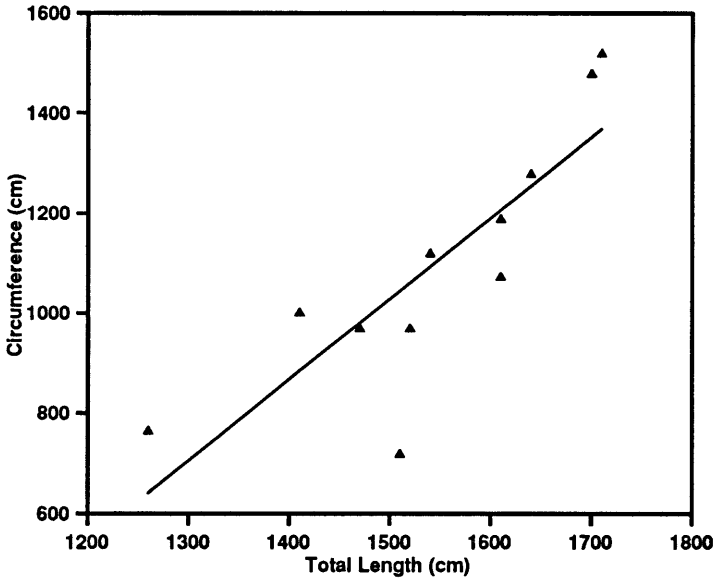

Figure 54: Linear least square fit plot of circumference at umbilicus

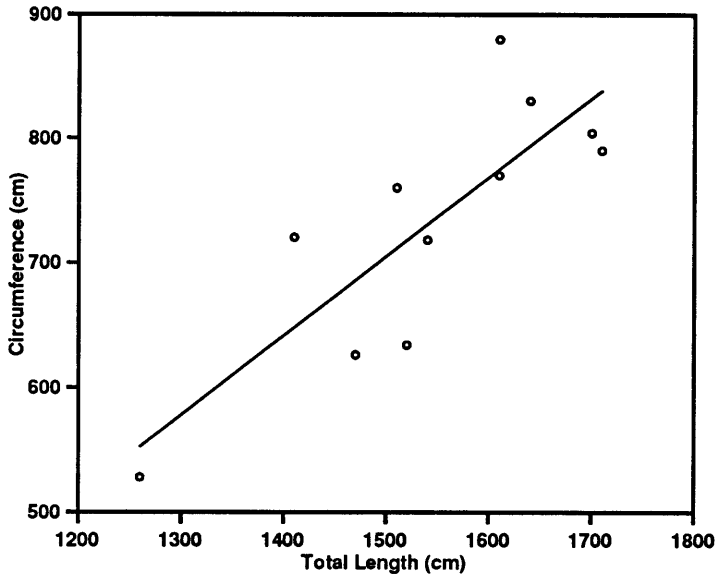

Figure 55: Linear least square fit plot of circumference at anus

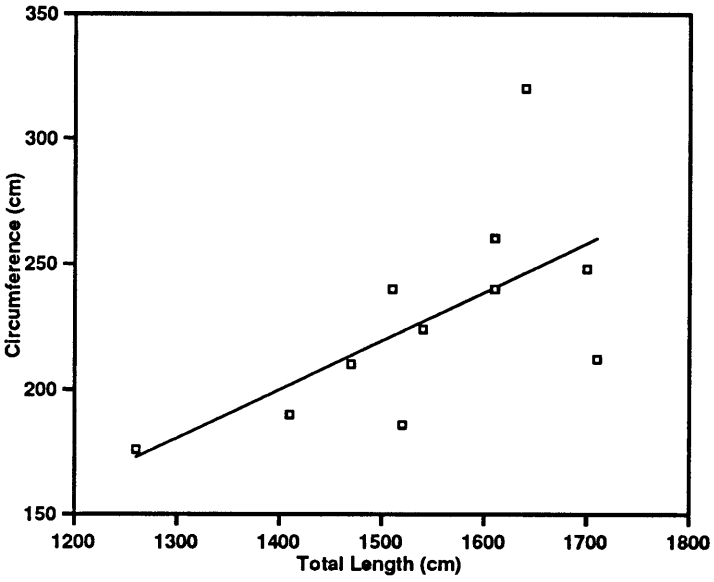

Figure 56: Linear least square fit plot of circumference at caudal terminus

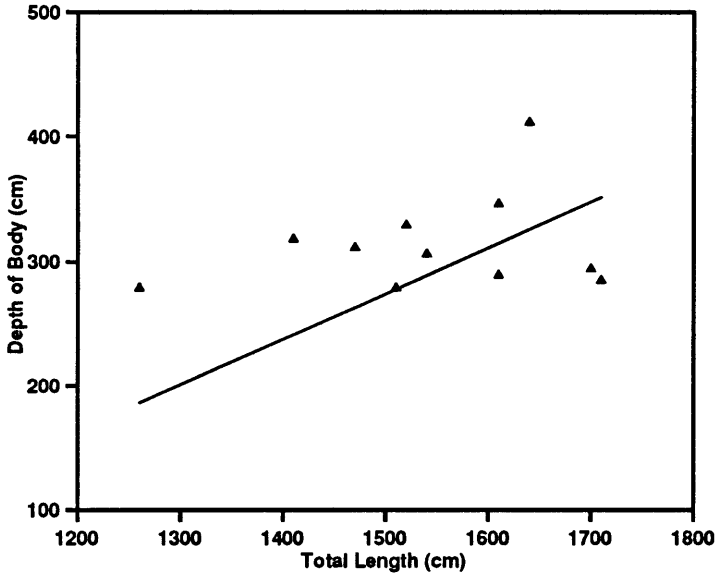

Figure 57: Linear least square fit plot of depth of body at umbilicus

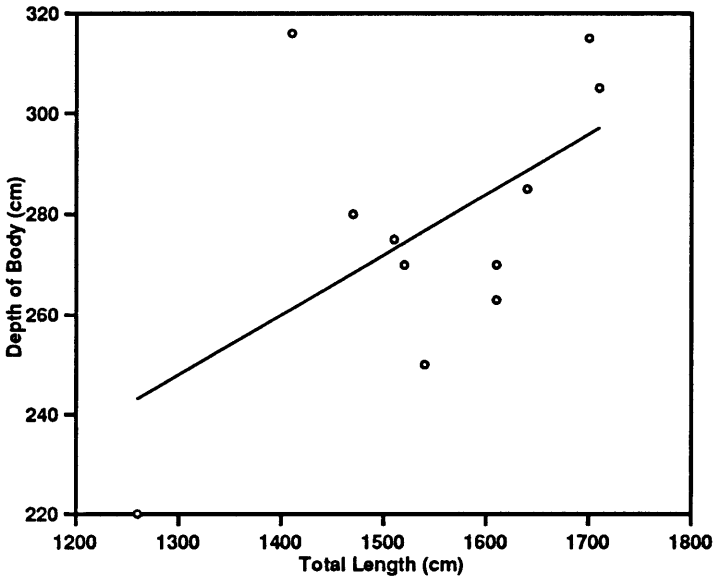

Figure 58: Linear least square fit plot of depth of body at anterior insertion of flipper

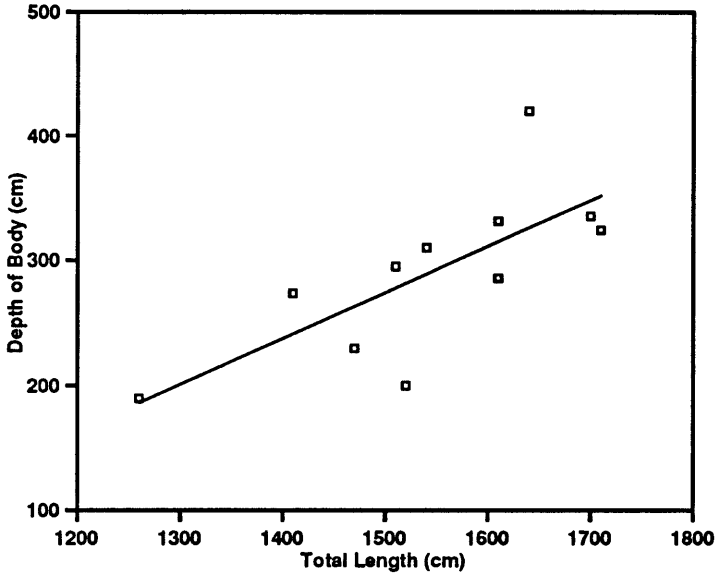

Figure 59: Linear least square fit plot of depth of body at middle insertion of flipper

Averages of Whale Measurements (cm)

Total Length.....	1543.6
Tail Flukes, Total Spread.....	543.5
F., Greatest Width.....	152.1
Circumference in Front of Flipper..	1053.3
Circumference at Umbilicus.....	1099.3
Circumference at Anus.....	732.7
C. at caudal Terminus or "small"..	227.8
Depth of Body at Umbilicus.....	314.4
D.o.B. at Middle Insertion of Flipp.....	290.4
D.o.B. at Anterior Insertion of Fli.....	277.2

Figure 60: Table of averaged whale dimensions pertinent to hydrodynamics and whale design

Appendix 1: Normalization of Whale Measurements to Create The Average Right Whale

Method

In order to perform simulations involving a right whale, an accurate geometric representation of the whale is developed. The data used to describe a typical right whale (Eubalaena Glacialis) are obtained from Omura *et al.* 1969. The following data are normalized with respect to the total length of the whale.

- Tail flukes, total spread.
- Flipper, greatest width.
- Circumferences at: front of flipper, umbilicus, anus, and caudal terminus.
- Depths of body: middle insertion of flipper, anterior insertion of flipper and umbilicus.

A linear least-squares approximation is fit to the data providing equations for each of the geometric parameters as a function of the whale length. The raw data are also averaged to find the geometric description of the average whale.

Equations: linear least-squares fits

Figures 53 through 60 show the whale geometric data with the linear least-squares fits. The equations for the linear approximations to the data are as follows. Let x be the total length of the whale and let y be any desired dependent variable (*e.g.* circumference, depth of body, etc.) Then the equations, with units in centimeters are: for circumference at front of flipper

$$y = 1.46x - 1200., \tag{1}$$

for circumference at umbilicus

$$y = 1.62x - 1400., \tag{2}$$

for circumference at Anus

$$y = 0.634x - 246., \tag{3}$$

for circumference at caumtal terminus

$$y = 0.194x - 71.0, \tag{4}$$

for depth of body at umbilicus

$$y = 0.070x + 206., \tag{5}$$

for depth of body at anterior insertion of flipper

$$y = 0.367x - 276., \tag{6}$$

and for depth of body at middle insertion of flipper

$$y = 0.120x + 92.3. \tag{7}$$

Ocean engineers characterize the shapes of ships and bodies by various coefficients. The "block coefficient" is a measure of the fullness of a body. It is the ratio of the actual body volume to that of a parallelopiped with the same overall length, width, and depth. The block coefficient for the average whale is approximately .4 which means that it is a considerably less full shape than the typical ship. What we refer to as the "cross-sectional coefficient" is a variation on the ship-oriented "midship section coefficient." It is the ratio of the greatest cross-sectional area to that of a rectangle of the same overall width and depth. The cross-sectional coefficient for the average whale is approximately .84 which is a typical value for a submarine and is approximately the value for a circle inscribed in a square ($\pi/4$).

Appendix 2: The Hydrodynamic Forces on Interacting Bodies, When Both Bodies Are Allowed to Move

Introduction

Modeling of hydrodynamic interactions in the presence of a free surface requires some simplifications in order to make the computations tractable. The primary simplification for this study is that the effect of free-surface waves created by the ship is not included. This is appropriate for ship speeds which are small compared to the maximum theoretical speed for the hull or where the body on which the forces are to be computed is submerged some distance below the free surface. The waves will have a small effect compared to the added-mass effect if their amplitude is small (due to low ship speed) or their effect is mitigated by depth (the affected body is submerged). Another simplification is that bodies or appendages will not create lift. This is appropriate as we do not expect to generate cross flow on the ship hull and we do not attempt to maneuver the whale by the thrust of the whale's flukes or fins. The fluid flow, then, may be modeled as the irrotational flow of an ideal fluid, with a scalar velocity potential which is a function of space and time.

The boundary value problem for this potential is solved numerically at each time step, the forces on the whale are computed, and the whale is accelerated subject to these forces. The details of these computations are provided in the following sections.

Derivation of the force expression

Regardless of how the potential flow problem is solved, the hydrodynamic force and moment acting on a body are evaluated as the integrals of the product of the pressure and the generalized normal vector over the body surface. After substituting for the pressure from Bernoulli's equation, we obtain

$$F_i = -\rho \int\int_{S_B} \left(\frac{\partial \phi}{\partial t} + \frac{1}{2} \nabla\phi \cdot \nabla\phi \right) n_i dS, \tag{8}$$

where S_B denotes the union of the bodies' wetted surface, since n_i is nonzero only on the body for which the mode i is defined. Direct evaluation of (8) requires the partial derivative with respect to time of the velocity potential, which is awkward to evaluate numerically if the body is moving. Therefore, to evaluate $\partial\phi/\partial t$, an approach which follows from the substantial derivative yields:

$$F_i = -\rho \frac{d}{dt} \int\int_{S_B} \phi n_i dS + \rho \int\int_{S_B} \left((U \cdot \nabla\phi) n_i - \frac{1}{2} \nabla\phi \cdot \nabla\phi n_i \right) dS, \tag{9}$$

where the vector U denotes the bodies' velocities. For the special case of one body moving and one body fixed, we can use the transport theorem, with the result:

$$F_i = -\rho \frac{d}{dt} \int\int_{S_B} \phi n_i dS + \rho \int\int_{S_B} \left(\frac{\partial \phi}{\partial n} V_i - \frac{1}{2} \nabla\phi \cdot \nabla\phi n_i \right) dS, \tag{10}$$

where V_i is defined respectively as the i-th component of the fluid velocity vector $\nabla\phi$ or the cross-product $r \times \nabla\phi$, evaluated on the body corresponding to mode i and elsewhere on S_B $V_i = 0$. The direct evaluation of the first term of (9) and (10) may only be done numerically by one-sided finite difference, because the positions of the bodies at the next time-step are not known before the forces are computed. A complementary expression for the force and moment may be derived from the Lagrangian analysis (Milne-Thomson, 1955). If the fluid boundaries, including the free surface, are rigid, the force components are given by

$$F_i = -m_{ij}\dot{u}_j - u_j u_k \left(\frac{\partial m_{ij}}{\partial x_k} - \frac{1}{2} \frac{\partial m_{jk}}{\partial x_i} \right), \tag{11}$$

where m_{jk} is the added-mass tensor,

$$m_{jk} = \rho \int\int_{S_B} \phi_k n_j dS \tag{12}$$

in which ϕ_i represents the velocity potential due to a body motion with unit velocity in the i-th mode. Thus the total potential can be expressed as the sum $\phi = u_i \phi_i$. The attractive aspect of the Lagrangian formulation is that the force and moment are expressed strictly in terms of the added-mass coefficients, and evaluation the velocity

vector on the body surface is not necessary. In (11), the derivatives of the added-mass coefficients with respect to the position arise from the concept of virtual work. Numerically, the derivatives are taken by separately moving the bodies in every single mode of motion and calculating the differences of the added-mass coefficients. In our present case, this greatly increases the computational burden because both bodies are moved by the hydrodynamic forces in surge, sway and yaw.

However we can arrive at an alternative approach which takes advantage of both the Bernoulli equation and Lagrangian analysis. The derivation begins by expressing the first term in (9) in terms of the added-mass coefficients:

$$\rho\frac{d}{dt}\int\int_{S_B}\phi n_i dS = \rho\int\int_{S_B}\frac{d}{dt}\left(u_j\phi_j\right)n_i dS$$

$$= \rho\int\int_{S_B}\frac{du_j}{dt}\phi_j n_i dS + \rho u_j\int\int_{S_B}\left(\frac{d\phi_j}{dt}\right)n_i dS$$

$$= \rho\dot{u}_j\int\int_{S_B}\phi_j n_i dS + \rho u_j\frac{d}{dt}\int\int_{S_B}\phi_j n_i dS$$

$$= \dot{u}_j m_{ij} + u_j\frac{dm_{ij}}{dt}. \tag{13}$$

Furthermore, we can express (13) as

$$\rho\frac{d}{dt}\int\int_{S_B}\phi n_i dS = \dot{u}_j m_{ij} + u_j\frac{dm_{ij}}{dt}$$

$$= \dot{u}_j m_{ij} + u_j\frac{\partial m_{ij}}{\partial x_k}\frac{dx_k}{dt}$$

$$= \dot{u}_j m_{ij} + u_j u_k\frac{dm_{ij}}{dx_k} \tag{14}$$

From (14), it is clear that first term in (9) is equal to the sum of the first terms in (11). Substituting (13) in (9) yields:

$$F_i = -m_{ij}\dot{u}_j - u_j\frac{dm_{ij}}{dt} + \rho\int\int_{S_B}\left((U\cdot\nabla\phi)n_i - \frac{1}{2}\nabla\phi\cdot\nabla\phi n_i\right)dS. \tag{15}$$

The advantage of (15) is that we can use central finite differencing to evaluate the time derivative in the second term hardly increasing the computational work. The interpretation of the second term in (15) is made via the concept of virtual movement, in which the generalized coordinates of the system are considered to be incremented by an infinitesimal amount from the values they have at an arbitrary instant with time held constant. In (15), the infinitesimal incremental amount, which is the virtual displacement, is computed by adopting the velocity at that arbitrary instant. By moving the bodies with the positive and negative orientations of the velocity at each time-step,

there are two virtual positions which are not on the exact paths which the bodies may have. The time-derivative term in (15) is computed by performing the central finite difference of the added-mass coefficients at the two virtual positions.

If we use R_i to denote the integral term, we can rewrite (15) as

$$F_i = -m_{ij}\dot{u}_j - u_j\frac{dm_{ij}}{dt} + R_i \tag{16}$$

If we assume the center of added-mass and the center of gravity to be coincident, the equation of motion is

$$F_i + F_{ei} = m\dot{u}_i \tag{17}$$

where m denotes the mass of the body and F_{ei} denotes the given external forces other than the hydrodynamic force in the i-th mode. Combining (16) and (17) in order to eliminate F_i, we get twelve simultaneous equations which are

$$m\dot{u}_i + \dot{u}_j m_{ij} = -u_j\frac{dm_{ij}}{dt} + R_i + F_{ei}. \tag{18}$$

After using usual matrix operations to solve the twelve simultaneous equations, the unknowns, $\dot{u}_j$, in (18) are found and the hydrodynamic forces are computed by (16).

Solutions of the flow problems

In the previous section it is seen that we must solve a series of flow problems in order to compute the forces and moments on each body. The flow problems are solved under several assumptions outlined by Korsmeyer *et al.* (1993). The major assumptions are that the fluid is ideal and free-surface waves are neglected. Assume that at each time-step the entire flow can be described by a velocity potential $\phi(x)$ where x is a position vector in a fixed Cartesian coordinate system which has the $z = 0$ plane coincident with the fluid surface and the positive sense of the z-axis directed out of the fluid.

In the fluid domain, the velocity potential $\phi(x)$ satisfies Laplace's equation

$$\nabla^2\phi = 0. \tag{19}$$

Boundary conditions must be provided on the surface $S_F \cup S_C \cup S_B$, with generalized unit normal vector n, which encloses the computational domain. On the free surface the velocity potential $\phi(x)$ satisfies the "rigid lid" boundary condition

$$\frac{\partial\phi}{\partial z} = 0 \quad \text{on } S_F, \tag{20}$$

on any boundary surface S_C which encloses the fluid, the velocity potential $\phi(x)$ satisfies the condition

$$\frac{\partial\phi}{\partial n} = 0 \quad \text{on } S_C \tag{21}$$

and on any moving-body surface S_B the velocity potential $\phi(x)$ satisfies the condition

$$\frac{\partial \phi}{\partial n} = U \cdot n \quad \text{on } S_B. \tag{22}$$

Applying Green's theorem gives the equation for the potential $\phi(x)$

$$2\pi\phi(x) + \int\int_{S_B \cup S_C} \phi(\xi) \frac{\partial}{\partial n_\xi} G(x;\xi) dS_\xi = \int\int_{S_B \cup S_C} G(x;\xi) \frac{\partial}{\partial n_\xi} \phi(\xi) dS_\xi, \tag{23}$$

and the equation for the source strength $\sigma(x)$

$$2\pi\sigma(x) + \int\int_{S_B \cup S_C} \sigma(\xi) \frac{\partial}{\partial n_x} G(x;\xi) dS_\xi = U \cdot n(x), \tag{24}$$

from which the the fluid velocity is given by

$$\nabla\phi(x) = 2\pi n(x)\sigma(x) + \int\int_{S_B \cup S_C} \sigma(\xi) \nabla_x G(x;\xi) dS_\xi. \tag{25}$$

In these equations $x \in S_B \cup S_C$. If S_C describes an enclosing surface with a rectangular cross-section then a particular Green function which satisfies (21) may be used to greatly reduce the computational effort (Newman, 1992).

Computational method

A panel method method is used to solve the potential problem at each time-step. In this method, the boundary surfaces are divided into N plane quadrilateral or triangular panels over which the strengths of the singularities are assumed to be unknown constants. After discretization, the integral equation becomes a linear system which may be solved by a direct or an iterative method.

Because the bodies are not fixed, we need to update the positions of the bodies at each time-step, with the acceleration of the bodies caused by the hydrodynamic forces calculated by (18) after solving the potential problems.

There are two different kinds of time-steps for the calculation of the hydrodynamic forces and motions. The primary kind of time-step we simply call the "time-step" and it controls the accuracy of motion. The other kind of time-step we call the "sub-time-step" and it controls the accuracy of the hydrodynamic force computation.

So using the sub-time-step, the discretized form of the time derivative term in (18) is given by

$$u_j \frac{dm_{ij}}{dt} = \frac{\rho u_j \sum_{k=1}^{N} (\phi_{jk}^{t+\Delta\epsilon} - \phi_{jk}^{t-\Delta\epsilon}) n_{ik} A_k}{2\Delta\epsilon}, \tag{26}$$

where $k, N, A, \Delta\epsilon$ denote the k-th panel, the number of panels, the area of the panel, and the magnitude of the sub-time-step, and $t = M\Delta t$ where M and Δt denote the M-th time-step and the magnitude of the time-step. Because (18) is solved in the body

coordinate system and rigid-body motions are assumed, the generalized normal vectors and the surface areas of the panels will not change with respect to time.

After solving (18), the forces may be obtained by (16). The evaluated forces and added-mass coefficients are non-dimensionalized by the appropriate combinations of water density ρ, body velocity U, and body length L. The non-dimensionalization is as follows:

The added-mass:

$$m_{ij} = \frac{\tilde{m}_{ij}}{\rho L^k} \tag{27}$$

The forces (and moments) whether the quadratic force or the total force:

$$F_{i,j} = \frac{\tilde{F}_{ij}}{\frac{1}{2}\rho U^2 L^m} \tag{28}$$

In these expressions, the tilde denotes dimensional quantities, and i, j are mode indices. In (27) and (28), $k = 3$ and $m = 2$ for $i, j = 1, 2, 3, 7, 8, 9$, $k = 5$ and $m = 4$ for $i, j = 4, 5, 6, 10, 11, 12$, and $k = 4$ and $m = 3$ for the other combinations.

After solving (18), the displacement is given by

$$D_i^t = u_i^t \Delta t + \frac{1}{2}\dot{u}_i^t (\Delta t)^2. \tag{29}$$

As mentioned above, the bodies are moved to two virtual positions at each time-step. If we use subscripts, o, $+$, $-$,to denote the exact position and two virtual positions moved from the exact position by positive and negative velocity respectively, those displacements are given by

$$P_+^t - P_o^t = u^t \Delta\varepsilon, \tag{30}$$

and

$$P_-^t - P_o^t = -u^t \Delta\varepsilon, \tag{31}$$

where P and u denote the position vector and the velocity vector, respectively. If the body is moved from P_+^t to $P_-^{t+\Delta t}$, we can take advantage of (29), (30), and (31)

$$\begin{aligned} P_-^{t+\Delta t} - P_+^t &= (P_-^{t+\Delta t} - P_o^{t+\Delta t}) + (P_o^{t+\Delta t} - P_o^t) + (P_o^t - P_+^t) \\ &= -u^{t+\Delta t}\Delta\varepsilon + u^t \Delta t + \frac{1}{2}\dot{u}^t (\Delta t)^2 - u^t \Delta\varepsilon. \end{aligned} \tag{32}$$

Between $u^{t+\Delta t}$ and u^t, the relation is given by

$$u^{t+\Delta t} = u^t + \dot{u}^t \Delta t. \tag{33}$$

Combining (32) and (33) in order to eliminate u^t, we can get

$$P_-^{t+\Delta t} - P_+^t = -u^{t+\Delta t}\Delta\varepsilon + u^{t+\Delta t}\Delta t - \dot{u}^t (\Delta t)^2 - u^{t+\Delta t}\Delta\varepsilon + a^t \Delta t \Delta\varepsilon$$

$$= u^{t+\Delta t}(\Delta t - 2\Delta\varepsilon) - \frac{1}{2}(\Delta t - 2\Delta\varepsilon). \tag{34}$$

Observing (34), the two positions, P_+^t and $P_-^{t+\Delta t}$ are identical and the computation is reduced if we choose the magnitude of the sub-time-step to be equal to one half of the magnitude of the time-step.

Appendix 3: Inclusion of Propeller Forces

The inclusion of a propeller behind the ship hull modifies the velocity potential so that the forces experienced by the whale are slightly different from the case with no propeller. The complete model of the flow due to the presence of a propeller is too complex for this analysis so we choose to model the propeller in the simple form of an actuator disk (Hough and Ordway, 1964). In this case, the fluid velocity due the the propeller is modeled in a way which is valid except very near to the propeller and in the propeller wake. The change in the added-mass terms for the ship and whale due to the presence of the propeller is expected to be negligible and is not included. From any point of view, the effect on the flow due to the presence of a propeller is small because the propeller acts like a disk of normal dipoles and the magnitude of the velocity due to a disk of normal dipoles decreases with the square of the distance from the disk.

This simple representation of the propeller is as a disk of zero thickness with a diameter equal to that of the propeller. Through the disk, the flow passes continuously while subjected to a constant pressure jump across the disk. The effects of a finite number of blades and the production of fluid rotation are ignored.

Under such an idealization, expressions have been developed for the velocity induced at radius r_c and axial position x_c by an infinite set of helical vortices uniformly distributed around the circumference of a circle of radius r_v. Replacing the Z concentrated vortices of unit strength (one for each blade) with a continuous distribution with total circulation Z is a simplification which allows a closed form to be found in terms of elliptic integrals. For a propeller with Z blades, pitch angle β, and thrust coefficient C_T, the axial velocity $\bar{u}_a$ and tangential velocity $\bar{u}_t$, which are the velocities normalized by the circulation Γ may be computed from:

for $r_c < r_v$

$$\bar{u}_a(x_c, r_c, r_v) = \frac{Z}{4\pi}\left(\frac{1}{\pi r_v \tan\beta} C_1\right)$$

$$\bar{u}_t(x_c, r_c, r_v) = \frac{Z}{4\pi}\left(\frac{1}{\pi r_c} C_2\right); \tag{35}$$

for $r_c > r_v$

$$\bar{u}_a(x_c, r_c, r_v) = \frac{Z}{4\pi}\left(\frac{1}{\pi r_v \tan\beta} C_2\right)$$

$$\bar{u}_t(x_c, r_c, r_v) = \frac{Z}{4\pi}\left(\frac{1}{\pi r_c} C_1\right); \tag{36}$$

where

$$C_1 = \pi + \frac{x_c}{2\sqrt{r_c r_v}} Q_{-\frac{1}{2}(q)} + \frac{\pi}{2}\Lambda_0(s,t)$$

$$C_2 = \frac{x_c}{2\sqrt{r_c r_v}} Q_{-\frac{1}{2}(q)} - \frac{\pi}{2}\Lambda_0(s,t); \tag{37}$$

and

$$q = 1 + \frac{x_c^2 + (r_c - r_v)^2}{2 r_c r_v}$$

$$s = \sin^{-1}\left(\frac{x_c}{\sqrt{x_c^2 + (r_c - r_v)^2}}\right)$$

$$t = \sqrt{\frac{4 r_c r_v}{x_c^2 + (r_c + r_v)^2}}\ . \tag{38}$$

Here, $Q_{-\frac{1}{2}}$ is the Lengendre function of the second kind and half integer order, and Λ_0 is the Heumann's Lambda function.

Each velocity component induced by the propeller is the product of $\bar{u}_a$ or $\bar{u}_t$ with the circulation computed from

$$\Gamma = 2\pi \frac{r_v}{Z} \tan\beta \left(\frac{C_T}{1 + \sqrt{1 + C_T}}\right). \tag{39}$$